sustainability

MDPI

Article

Time History Analyses of a Masonry Structure for a Sustainable Technical Assessment According to Romanian Design Codes

Vasile-Mircea Venghiac [1], Cerasela-Panseluta Neagu [1], George Taranu [1,*] and Ancuta Rotaru [2]

[1] Department of Structural Mechanics, Faculty of Civil Engineering and Building Services, Technical University "Gheorghe Asachi" of Iasi, 1 Prof. Dr. Doc. Dimitrie Mangeron St., 700050 Iași, Romania
[2] Department of Transportation Infrastructure and Foundations, Faculty of Civil Engineering and Building Services, Technical University "Gheorghe Asachi" of Iasi, 1 Prof. Dr. Doc. Dimitrie Mangeron St., 700050 Iași, Romania
* Correspondence: george.taranu@academic.tuiasi.ro

Abstract: Computer simulations are challenging in terms of modeling the appropriate behavior of brick masonry structures. These numerical simulations are becoming increasingly difficult due to several design code requirements considered for the technical assessment of brick masonry structures for rehabilitation. In Romania, many brick masonry structures have withstood powerful earthquakes during their lifetime and require rehabilitation works. This paper aims to further assess various simulation challenges regarding the boundary conditions of spandrels and masonry structural behavior. This paper presents a comparative numerical study of two different spandrel-piers scenarios: one considers the link between them as unaffected, and the other attempts to simulate the occurrence of damage by replacing the spandrel's presence in the initial structure. The proposed model follows the "strong pier–weak spandrel model" and is aimed at practicing engineers. Models are computed with ordinary design software such as Robot Structural Analysis with 2D shells finite elements for masonry walls and, in a more complex manner, software such as Ansys with 3D solid finite elements. Time history analyses are carried out for three distinct accelerograms recorded in Romania. A comparison of the results acquired from these two models is presented and discussed. The purpose of this research is to highlight the importance of proper modeling of unreinforced brick masonry structures to optimize operational and maintenance practices.

Keywords: time history analyses; brick masonry spandrel modeling; solid brick masonry structures; sustainable retrofitting techniques; life cycle monitoring

check for updates

Citation: Venghiac, V.-M.; Neagu, C.-P.; Taranu, G.; Rotaru, A. Time History Analyses of a Masonry Structure for a Sustainable Technical Assessment According to Romanian Design Codes. *Sustainability* **2023**, *15*, 2932. https://doi.org/10.3390/su15042932

Academic Editors: Humberto Varum and Claudia Casapulla

Received: 30 December 2022
Revised: 20 January 2023
Accepted: 1 February 2023
Published: 6 February 2023

Copyright: © 2023 by the authors. Licensee MDPI, Basel, Switzerland. This article is an open access article distributed under the terms and conditions of the Creative Commons Attribution (CC BY) license (https://creativecommons.org/licenses/by/4.0/).

1. Introduction

The extended meaning of sustainability refers to the ability of something to maintain or "sustain" itself over time.

The construction industry impacts all four aspects of sustainable development: ecological, economic, social, and cultural.

The main goal of sustainable development is to preserve the ecological systems that are, globally, the basis for human life and nature's biodiversity.

The challenges of the construction sector are the use environmentally friendly construction materials, the energy efficiency of buildings, reuse of construction and demolition waste materials, water conservation and health in structures, building-related transport aspects, urban sustainability, and societal impacts arising from construction activities and the built environment [1]. The main reasons for difficulties are the political, technological, and cultural differences between countries. They originate in the dependence of a subjective evaluation applied to each general method developed so far.

While the definition of sustainable building design is ever-changing, the National Institute of Building Sciences, established by the United States Congress, defines six fundamental principles that involve sustainability in the building industry: optimize site

potential; optimize energy use; protect and conserve water; optimize building space and material use; enhance indoor environmental quality (IEQ); optimize operational and maintenance practices [2].

Consuming vast amounts of materials and being a significant producer of harmful gases because of the raw materials and energy provided by non-renewable sources, the construction industry faces a new challenge. It meets increasing demands for new or renovated sustainable building designs balanced with safe, secure, and effective environments.

One of the main tasks of the civil engineer, faced with assessing the state of an old structure, is to find solutions for its rehabilitation to increase its service life. This leads to significantly less disruptions in the activities taking place in the building, reduced relocation periods for the inhabitants, and significantly less wastes, rather than demolishing the structure and building it again.

Through collaboration, engineers, architects, and other site contractors can specify materials and systems that simplify operational practices and reduce maintenance requirements. On site and within the facility, these practices, apart from reducing water and energy requirements and demanding less toxic chemicals usage, are cost-effective and reduce life-cycle costs. It is imperative to create strategies for sustainable development, especially for the rehabilitation of old urban areas [3].

Great interest is applied to the rehabilitation of the built environment. The concept of rehabilitation of old urban areas allows the achievement of sustainable development since it provides the use of existing structures, avoids the increase of constructed zones, and provides reduction of material consumption and waste production. It also sustainably preserves the regional cultural heritage [3].

The majority of old or historical buildings that require rehabilitation are masonry structures. Brick masonry structures are complex systems [4]. The complexity comes from the inhomogeneity of the material. The geometry variation can also create design difficulties [5]. All these issues create great challenges for structural engineers. The design process is also affected by different types of degradations. In the design process, the degradations are considered by means of safety factors, which reduce certain mechanical characteristics of the materials, such as compressive strength and modulus of elasticity.

Two main structural elements are identified in a masonry wall: the vertical panels, known as piers; and the horizontal elements which couple two adjacent piers, known as spandrels. The piers are the most important elements, being subjected to both static and seismic loads [6].

International codes, such as FEMA 356 [7], propose two simplified models: the "strong pier–weak spandrel" model; and the "strong spandrel–weak pier". Generally, the strong spandrel–weak pier model is consistent with new buildings in which the spandrels are always connected to lintels, tie-beams, and slabs, which provide a consistent coupling between the piers. As a consequence, the piers crack first. However, this is not always true for old or historic buildings where the spandrels are weak elements. The lintels in this case are usually made of wood or masonry, the tie-beams are either missing or made of wood and the floors are also made of wood [8].

According to [9,10] two types of cracking patterns were observed in masonry spandrels: flexural cracking patterns; and shear cracking patterns. These failure modes are generally related to spandrel geometric proportions, lintel type, and brick interlocking at the end-sections [9–12]. Slender spandrels typically fail in flexural mode while squat spandrels fail because of shear.

More complex modeling methods, analysis methods, and elaboration of analysis results can be used for accurate results, such as the derivation of analytical capacity curves and fragility functions [13], non-linear static analysis procedures [14–17], equivalent frame model [18,19]; or for identifying the weakest component, such as the component method for steel structures [20], the capacity design rule [19,21]. However, these methods are overly complex and impractical for practicing structural engineers, who require time-efficient models rather than very high-accuracy ones.

In Romania, the technical assessment of existing buildings is being performed in accordance with the provisions of Code P100-3/2019. The procedure is explained in Chapter 2. The hand calculations presented in the code are simplified to reduce complexity. However, for complex buildings, with many structural elements to be assessed, the procedure becomes difficult, and the risk of human error is high. In this paper, the authors propose a simplified numerical model for assessing the design pier forces in masonry structures. The scientific contribution of the study presented in the article is an approach to numerical models based on previous work [22–26]. Observations during the shaking table tests presented in Figure 1 show that the initial structural masonry wall transforms into the mechanism shown in Figure 2.

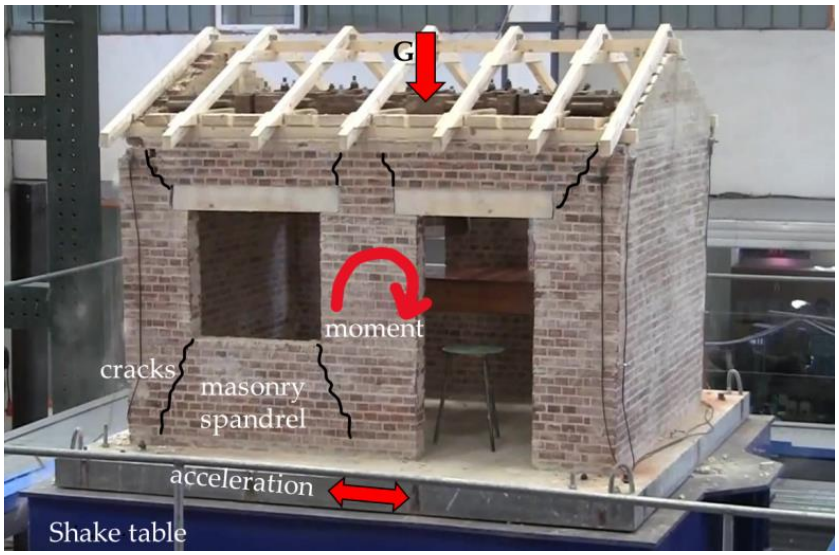


Figure 1. Mechanism of a 1:2 scaled unreinforced masonry structure model tested on the shaking table test [27,28].

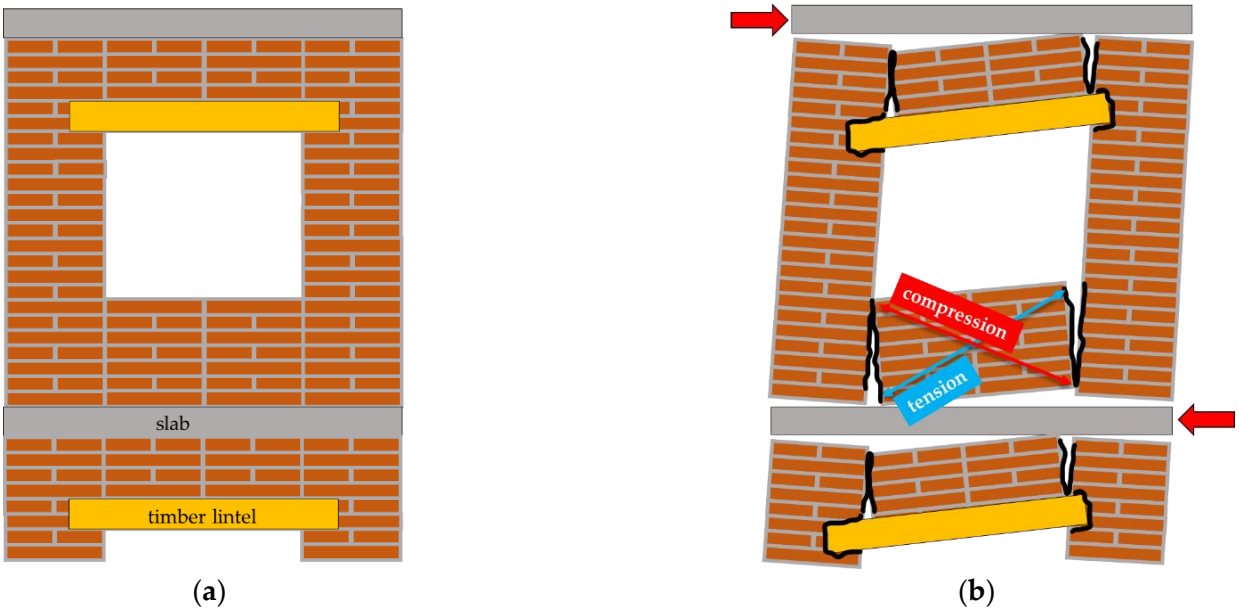


Figure 2. Masonry wall with window hole: (**a**) undeformed shape; (**b**) rocking mechanism during seismic action.

Finite elements models are considered as 3D solids and 2D shells in linear and nonlinear behavior. The material is considered homogeneous in both cases. The hypothesis in approaching the finite element models consists in a continuous rigid double-hinged

spandrel model used for unreinforced brick masonry, following the strong pier–weak spandrel model as shown in Figure 2. The proposed model is intended for slender spandrels rather than squat ones, which are also not connected to lintels, tie-beams, and floors. The models were subjected to three of the most important earthquakes which occurred and were recorded in Romania. The Vrancea region of Romania, the epicenter of the large tectonic earthquakes associated with Eastern Europe, has experienced a series of earthquakes with magnitudes over 6 degrees on the Richter scale in the past decades, namely: in 1977—M = 7.4; in 1986—M = 7.1 and 1990—M = 6.7 [25].

Table 1 shows the major earthquakes recorded in the Vrancea region and their particularities.

Table 1. Characteristics of major recorded earthquakes in the Vrancea region.

No.	Earthquake–Magnitude	LatN	LongE	h(km)	Date	Mw
1	Vrancea M= 7.2	45.34	26.30	109	1977.03.04	7.5
2	Vrancea M = 7.0	45.53	26.47	133	1986.08.30	7.3
3	Vrancea M = 6.7	45.82	26.90	91	1990.05.30	7.0
4	Vrancea M = 6.1	45.83	26.89	79	1990.05.31	6.4
5	Vrancea M = 6.0	45.79	26.71	100	2004.10.27	6.0

The finite element models proposed for designing rehabilitation solutions corresponds more closely to the real behavior of masonry structures than the analytical model proposed by the P100-3/2019 [29]. The latter method overestimates the values of internal forces in the structure. Moreover, by using a computer software technique, the accuracy of the results is higher than hand calculations. Another benefit of automatic calculation is time efficiency and the possibility of running a complex parametric analysis.

2. Materials and Methods

The Romanian code P100-3/2019 presents evaluation and estimation methods of the design forces produced by earthquakes (axial force, shear force, bending moments). The approaches presented in the code are simplistic in terms of the real structural behavior and that is because the process needs to be time-efficient. Some of the formulae do not consider all parameters required to do an accurate estimation, being the reason for the discussions presented in the annexes regarding the errors encountered in the design process.

The assessment is carried out according to one of three methodologies presented in the code. The methodology is chosen based on building importance class, site characteristics, an available information about the construction, such as preliminary technical project, year of construction, structural system, and material characteristics. The first level methodology is the simplest one ("low complexity"), and it is based on evaluating the ratio between the overall shear capacity of the building and the total base shear force. This methodology is rarely used because it is targeted at low-importance class buildings located in areas with low seismic impact (class of importance and seismic exposure III and IV as per P100-1/2013), and which comply with strict regularity and structural layout conditions.

Level 2 and 3 methodologies are considered advanced and may be applied to all types of structures. The assessment is conducted by evaluating the ratio between the sum of shear capacities of all vertical structural elements and the total base shear force. The main difference between the two methodologies is that the second methodology, which is the most widely used procedure, uses linear static analysis, while the third uses non-linear analysis. In the linear static analysis, the degradations of the building are taken into account by means of safety factors which reduce certain mechanical characteristics of materials (e.g., compressive or tensile strength, modulus of elasticity).

The Romanian code stipulates that an appropriate methodology for the seismic assessment of an existing building has to be chosen based on building importance class, site characteristics including seismic hazard, and available information about the construction, defined by P100-3/2019 as the "level of knowledge", such as the initial technical project, year of construction, structural system, and material characteristics.

The levels of knowledge are defined in Section 4.3 of the P100-3/2019 code as follows: KL1—limited knowledge; KL2—normal knowledge; KL3—complete knowledge.

For masonry structures, the code P100-3/2019 stipulates (Annex D.3.1.(6)) that "the third level methodology can only be applied to buildings where, following data collection for the structural assessment, the level of knowledge is KL3".

The factors considered in establishing a complete knowledge level (KL3) are as follows: (a) the geometry of structure (determined from the original overall project and from a comprehensive survey of the building); (b) the composition of structural and non-structural elements; (c) the materials of the structural and non-structural elements. Points (b) and (c) are determined from the original technical design documentation, from the original reports on the quality of works, and from a comprehensive inspection in the field.

For old masonry buildings, many of which suffered the impact of repeated earthquakes, reaching the requirements imposed by KL3 level of knowledge is difficult/not possible in Romania [29].

For these reasons, the authors propose a simple numerical model for the technical assessment of the design pier forces in unreinforced masonry structures, using the second level methodology, namely, linear static analysis.

The second level methodology (Chapter D.3.3.1.4, P100-3/2019) presents the formulae for the bearing capacity of the structural walls. Only the in-plane loading carrying capacity was considered in this article.

The shear capacity for eccentric compression failure (Figure 3a), V_{f1}, is:

$$V_{f1} = \frac{N_d}{c_p \lambda_p}(1 - 1.15\nu_d), \tag{1}$$

where:

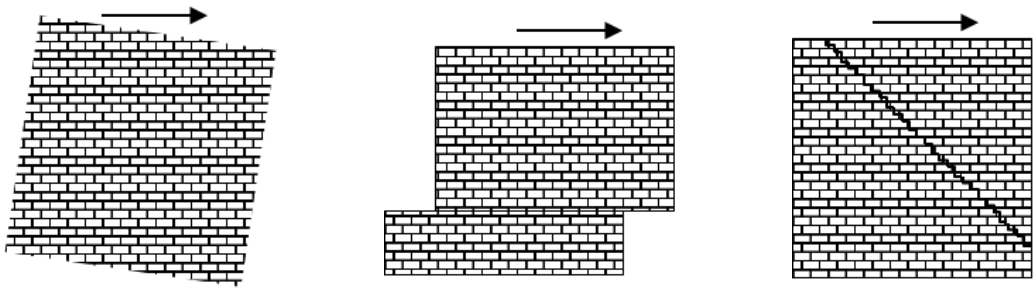


Figure 3. Masonry failure modes: (**a**) eccentric compression failure; (**b**) bed joint sliding; (**c**) diagonal shear cracking.

N_d is the design axial force;
c_p—coefficient which takes into account the bearing conditions at both ends of the pier;
$\lambda_p = \frac{H_p}{l_w}$—masonry wall shape factor;
H_p—height of the wall;
l_w—length of the wall;
$\nu_d = \frac{\sigma_0}{f_d}$ and $\sigma_0 = \frac{N_d}{A_w}$—vertical compression stress acting on the wall;
A_w—horizontal section area of the wall;
f_d—masonry design compression strength.

The shear capacity for bed joint sliding (Figure 3b), V_{f21}, is:

$$V_{f21} = \frac{1.33}{CF\gamma_M}\left(f_{vk0}\frac{l_{ad}}{l_c} + 0.4\sigma_d\right)tl_c, \tag{2}$$

where:

CF is the confidence factor;
γ_M—material partial safety coefficient;
f_{vk0}—initial characteristic shear strength of masonry;
t—thickness of the wall;
$l_{ad} = 2l_c - l_w$—length of active adherence;
$l_c = 1.5l_w - 3\frac{M_d}{N_d}$–length of compressed zone which takes into account the alternating effect of the seismic force;
M_d—design bending moment.
The shear capacity for diagonal shear cracking (Figure 3c), V_{f22}, is:

$$V_{f22} = \frac{tl_w f_{td}}{b}\sqrt{1 + \frac{\sigma_0}{f_{td}}}, \quad (3)$$

where:
f_{td} is the tensile strength of masonry;
b—coefficient computed according to: $1.0 \leq b = \lambda_p \leq 1.5$.
The shear capacity, V_{f2}, is:

$$V_{f2} = \min\left(V_{f21}, V_{f22}\right). \quad (4)$$

The design bearing capacity, V_{Rd}, is:

$$V_{Rd} = \min\left(V_{f1}, V_{f2}\right). \quad (5)$$

According to P100-3/2019, Chapter 8.1, three indicators (R_1, R_2, and R_3) establish the seismic risk class of the building. R_1 is a score based on the structural make-up of the building, R_2 is a score based on the structural degradations, and R_3 relies on the bearing capacity computation of the structure in the ultimate limit state. This paper considers only the R_3 indicator, evaluating it as follows:

$$R_3 = \frac{\sum V_{Rdi}}{\sum V_{Edi}}, \quad (6)$$

where:
V_{Rdi} is the design shear capacity in structural element i;
V_{Edi}—the design shear force in structural element i.
According to Chapter 8.1.3 of P100-3/2019, the seismic risk class associated to the R_3 indicator (expressed in %) is established as follows:

- seismic risk class Rs I, if $R_3 < 35\%$;
- seismic risk class Rs II, if $35\% \leq R_3 < 65\%$;
- seismic risk class Rs III, if $65\% \leq R_3 < 90\%$;
- seismic risk class Rs IV, if $R_3 \geq 90\%$ [22].

The first two risk classes (Rs I and Rs II) refer to buildings in danger of collapse and in need of structural rehabilitation. Class Rs III refers to buildings where non-bearing structural elements (partition walls, claddings) may be damaged, but structural collapse is unlikely. Class Rs IV refers to buildings that perform as expected under the design value of the seismic action, namely, new buildings.

3. Modeling of the Structure

3.1. Finite Element Model Description

The model analyzed in this case study is similar to that presented and computed in P100-3/2019 Annex H, using the specific provisions of the code. It is a 3-story residential building made of unreinforced solid brick masonry with RC slabs in 1925. The structure is asymmetrical in the plane as presented in Figure 4, but it has the same structural

layout on all levels as shown in Figures 5 and 6. There are no visible degradations from previous earthquakes.

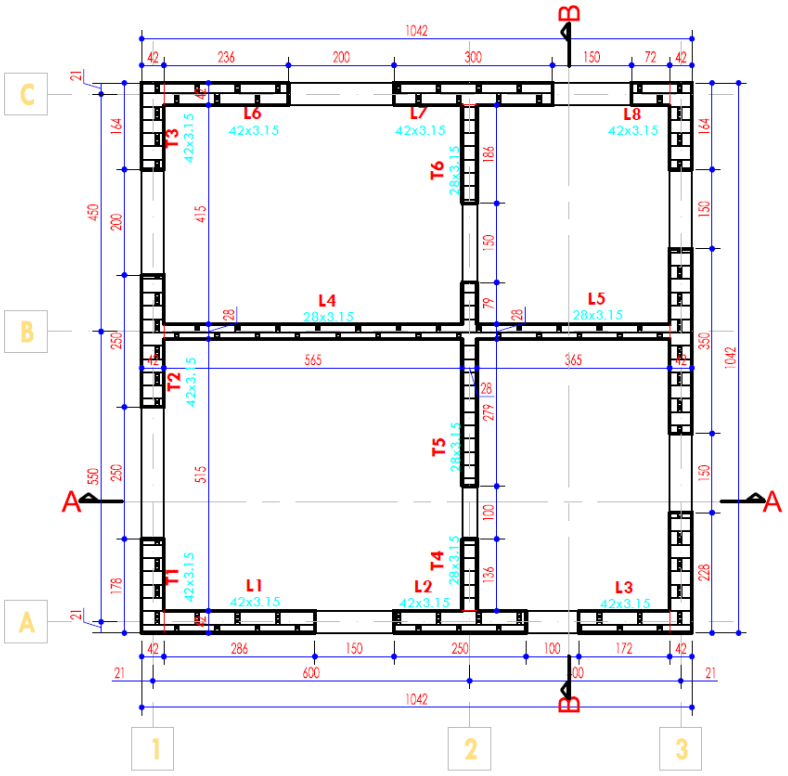


Figure 4. Floor plan with pier labels and building axes (longitudinal A, B, C and transversal 1, 2, 3).

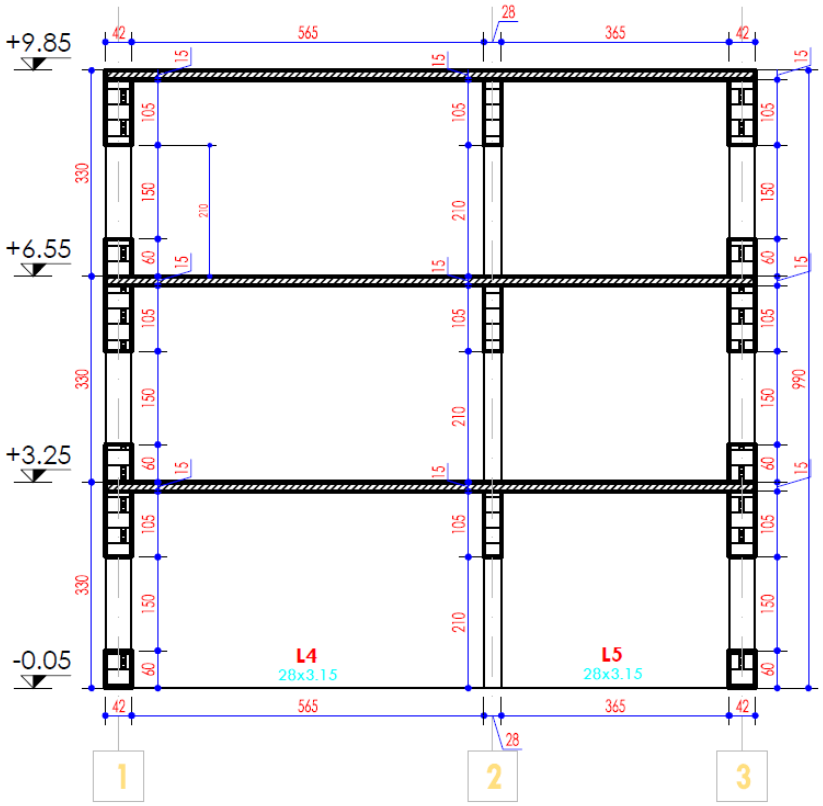


Figure 5. Section A-A with transversal building axes 1, 2, 3.

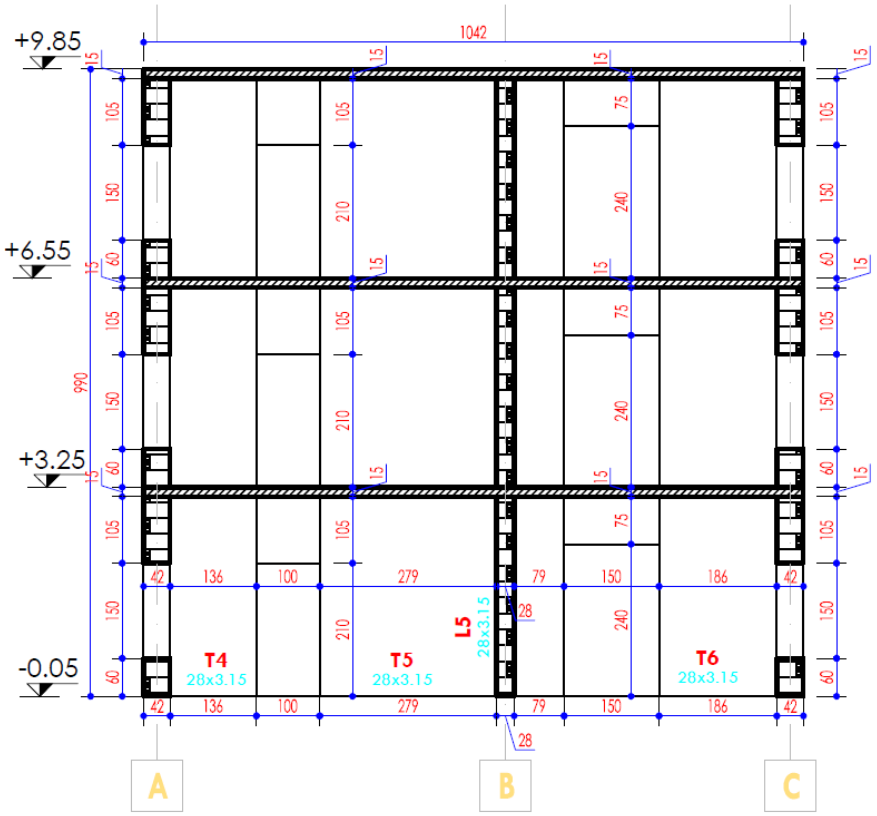


Figure 6. Section B-B with longitudinal building axes A, B, C.

There are no original plans or other technical documentation from the time of building completion, which leads to the second level of knowledge (KL2) according to P100/3-2019 Chapter 4.3 and adopting a confidence factor CF = 1.2.

The exterior wall thickness is 42 cm, and the thickness of the interior walls is 28 cm. The depth of the reinforced concrete slab is 15 cm. The story height is 3.3 m [29]. Figure 2 shows the floor plan dimensions (in centimeters) as they appear from the building survey.

Figure 3 presents mainmasonry failure modes for piers. The active piers along the *X*-axis are labelled L1 ÷ L9 and those along the *Y*-axis are labelled T1÷T9.

The two finite element software environments used for all simulations are Ansys [30] for the 3D non-linear model and Robot Structural Analysis for 2D linear models [31].

The article approaches two types of models, each one with two cases of structural integrity (initial and damaged).

All the finite element models ignore the lintels. The names of the FE models considered are given in Table 2.

Table 2. Description and names of the finite element models.

Recorded Seismic Action	2D Shell Linear		3D Solids Non-Linear	
	Bonded	Rigid Links	Bonded	Frictionless
Bucharest 1977	2D-L-B_Buc_77	2D-L-R_Buc_77	3D-NL-B_Buc_77	3D-NL-F_Buc_77
Bucharest 1986	2D-L-B_Buc_86	2D-L-R_Buc_86	3D-NL-B_Buc_86	3D-NL-F_Buc_86
Bucharest 1990	2D-L-B_Buc_90	2D-L-R_Buc_90	3D-NL-B_Buc_90	3D-NL-F_Buc_90

3.1.1. 2D Shells Linear Modeling

For the 2D shell model presented in Figure 7, the masonry piers and spandrels were the modelled with rectangular shell finite elements. The dimensions of elements are

210 × 210 mm. For concrete slabs, the element type is rigid diaphragm, because they are considered floor as part of the structure.

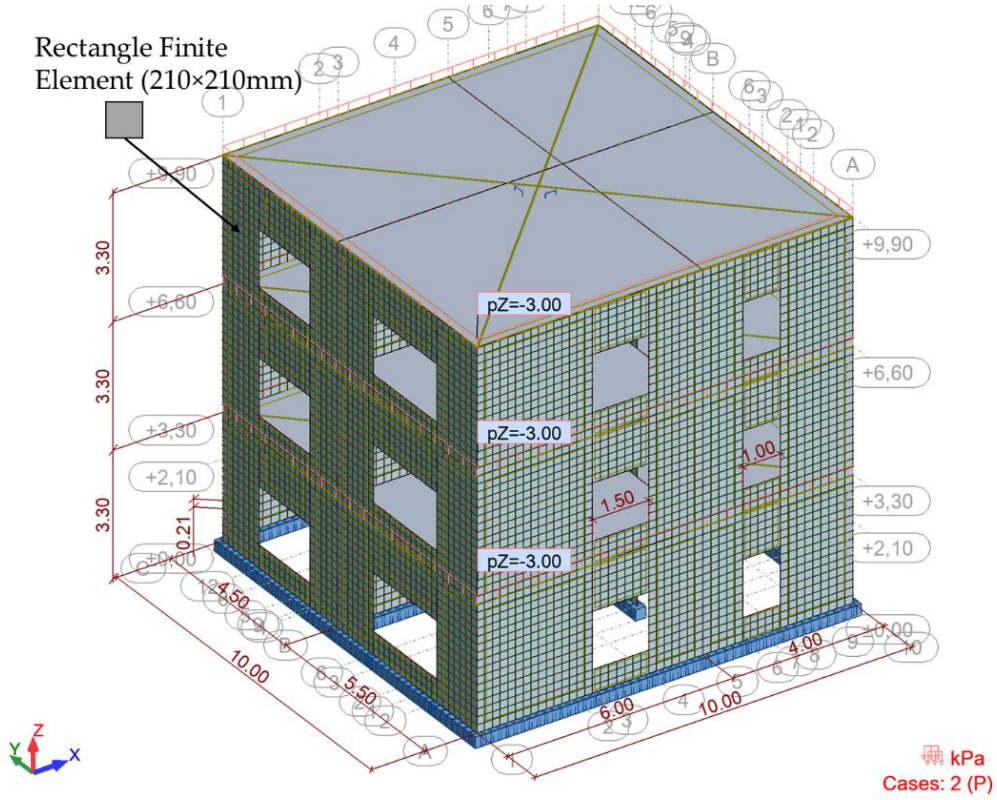


Figure 7. 2D shell linear model—bonded.

Simulations performed with this model are closer to the behavior of the weak pier–strong spandrel model. This is because the shells used to model the spandrels are fully connected to the piers. No additional boundary conditions were defined to simulate their detachment from the piers under seismic actions, and degradation in the spandrels was not considered. The total number of finite elements is 11,955, with a total number of nodes of 12,515.

The second 2D linear model discussed is called the 2D linear shell model, with rigid links instead of spandrels. It consists of brick masonry walls modeled with finite shell elements and brick masonry spandrels modelled with hinged rigid links, as shown in Figure 8.

The 2D linear model with rigid links is defined as double-hinged at the top and bottom of the window and door holes, as seen in Figure 8. These characteristics allow the rocking of the spandrel between two adjacent piers, simulating a weak link between the spandrel and piers. The hypothesis is that the spandrel does not provide any flexural stiffness. This hypothesis is true for many historic buildings which already show degradation in the spandrel area from previous earthquakes. Spandrels in this type of building are not connected to lintels, tie-beams, or floors. The total number of planar finite elements is 9984, with a total number of nodes of 10,538. The number of rigid links is 731.

The chosen arrangement of linear elements in the spandrels and their behavior under seismic actions are shown in Figure 8. This arrangement allows the spandrel to transmit loads between adjacent piers as in the diagonal compression strut model [8].

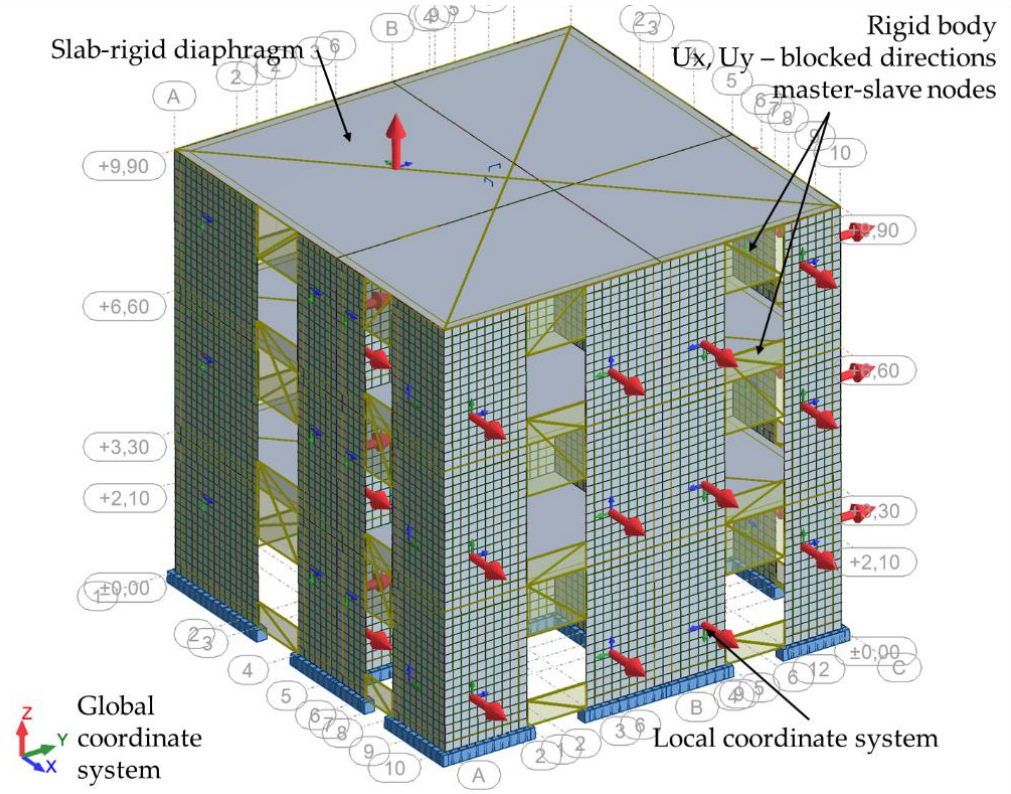
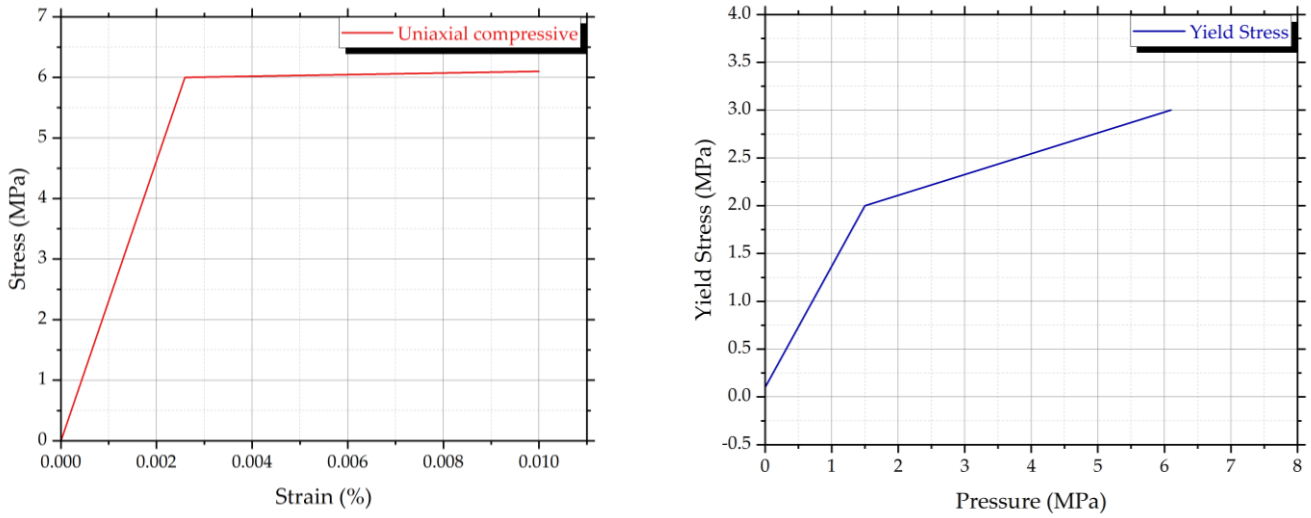


Figure 8. 2D shell linear model—rigid links.

3.1.2. 3D solid non-linear modeling

For the 3D solid model, two types of non-linearities were considered. One is for the homogenous masonry material with a uniaxial bilinear stress–strain curve in compression shown in Figure 9 and the second is based on the contacts between spandrels and piers which are frictionless with $\mu = 0$, presented in Figure 10a.



(**a**) (**b**)

Figure 9. Masonry homogenous material definition in Ansys: (**a**) uniaxial compressive; (**b**) Drucker–Prager Strength Piecewise yield criterion.

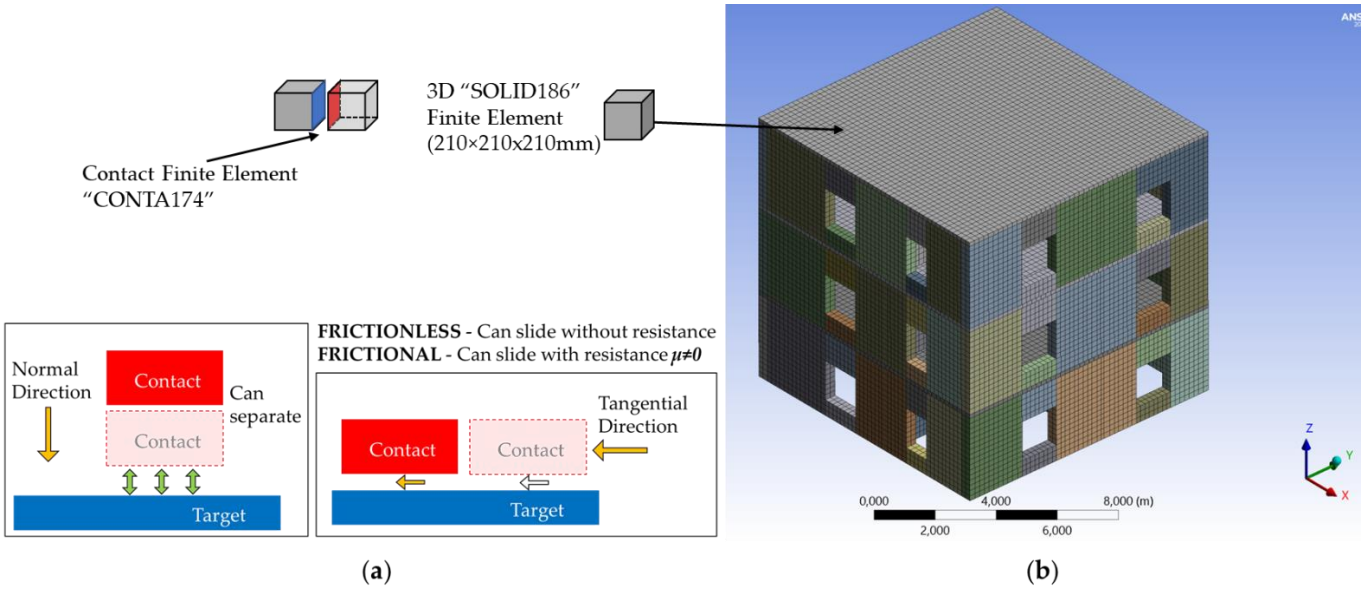


Figure 10. 3D solid model: (**a**) finite element units and contact definition: (**b**) mesh discretization of the 3D solid structural model.

In the frictional contact type setting, "the two contacting geometries can carry shear stresses up to a certain magnitude across their interface before they start sliding relative to each other. This state is known as "sticking." The model defines an equivalent shear stress at which sliding on the geometry begins as a fraction of the contact pressure. Once the shear stress is exceeded, the two geometries will slide relative to each other. The coefficient of friction can be any non-negative value" [32]. In case of frictionless contact type, the elements in contact can slide tangentially without resistance and the normal pressure equals zero if separation occurs. "Thus gaps can form in the model between bodies depending on the load. This solution is non-linear because the contact area may change under load. A zero coefficient of friction is assumed, allowing free sliding" [32].

The mesh discretization and the environment considered in the analyzed model are shown in Figure 10. The total number of solid elements is 31,578 with a size of 210 × 210 × 210 mm. The type of 3D solid elements is "solid186" and the type of contact is "conta174". The total number of the elements is 63,732.

Even though masonry is not a homogeneous material, the modeling process assumes that the material is homogenous for simplicity. This type of modeling, called macro-modeling [33,34], provides reasonable accuracy for stress and strain distribution in large structures. For the same reason, shell elements are considered linear in analysis. The macro-block model with 3D solid elements for masonry walls and the spandrel is based on the assumption that failure occurs at the interface between the spandrel and piers. To simulate this mechanism, tensionless and frictionless behavior is assumed at the interfaces (Coulomb failure criterion [35,36]). Masonry wall piers and spandrels are considered separated blocks. The aim of the numerical study was to observe the general tendency, model stiffness, and structural behavior in comparison with the 2D analysis. Therefore, the quantitative evaluation of stresses and the failure mechanism of the masonry walls were not investigated, considering the plastic behavior of masonry. Table 3 shows the properties of the materials used in all numerical models. Similar approaches of masonry structural systems were also used in the scientific literature [37–45].

3.2. Finite Element Loads Description

The applied loads presented in Figure 11 are described in Table 4.

The recorded accelerograms of the considered earthquakes are in the NS longitudinal direction. Figure 12 illustrates the time history accelerograms recorded for the previously mentioned earthquakes.

Table 3. Material properties used in the models.

Concrete Class C16/20	Density (kg/m^3)		2000
	Young's Modulus (MPa)		29,000
Masonry homogeneous material	Density (kg/m^3)		
	Isotropic elasticity	Derive from Young's modulus and Poisson's ratio	
		Young's modulus (MPa)	2310
		Poisson's ratio (MPa)	0.15
		Bulk modulus (MPa)	1100
		Shear modulus (MPa)	1004
	Uniaxial test data	Compressive stress–strain curve	Figure 9a
	Drucker–Prager strength piecewise	Yield stress–pressure curve	Figure 9b
	Tensile pressure failure	Maximum tensile pressure (MPa)	−0.1
	Crack softening failure	Flow rule	No Bulking
		Fracture energy Gf (J/m^2)	10

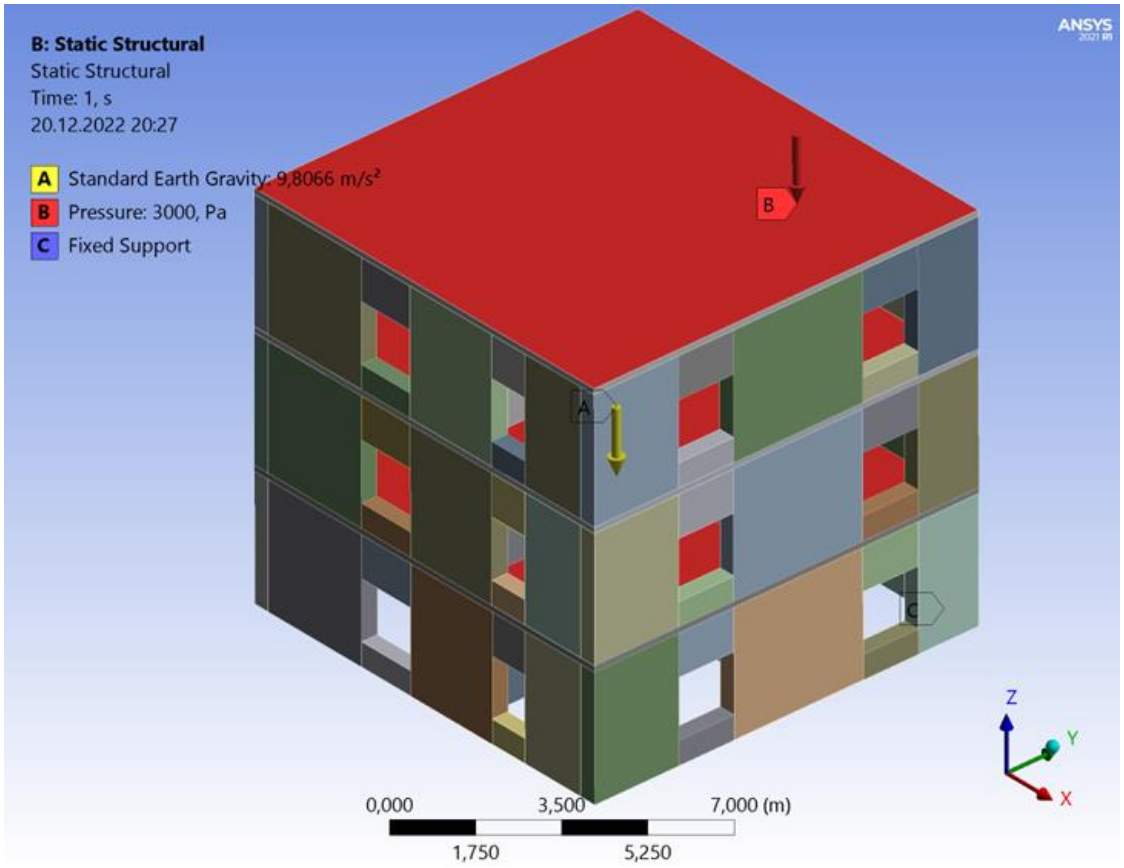


Figure 11. The applied loads on the 3D model.

Table 4. Applied loads [46].

Load Type	Load Name	Characteristic Load Value
Permanent	Self-weight:	
	- Masonry	18 kN/m^3
	- Reinforced concrete	25 kN/m^3
	Plaster 2 cm thickness	0.40 kN/m^2
	Levelling layer + Finishing	1.40 kN/m^2
	Partition walls	1.25 kN/m^2
Variable	Live load: people, furniture	1.50 kN/m^2

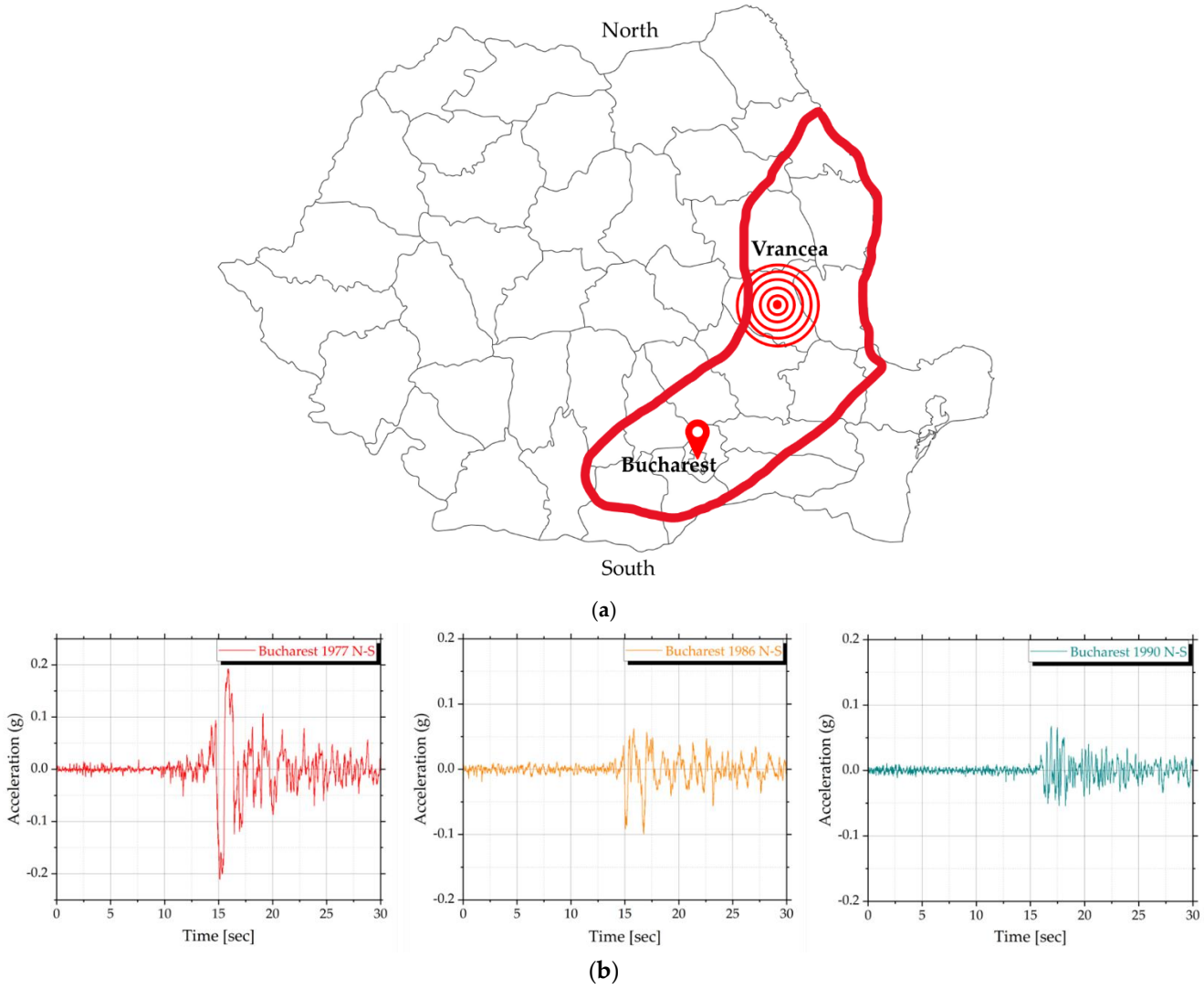


Figure 12. Romania Vrancea's earthquake: (**a**) N–S direction with Vrancea's epicenter and Bucharest capital; (**b**) time history recorded accelerograms in Bucharest, [47].

Time history analysis does not usually apply to assess the seismic response of structures in comparison to conventional methods such as response spectrum or modal analysis method because of the lack of knowledge and availability of the actual ground motion data inputs [48].

In this dynamic analysis, the method may apply the earthquake motion directly at the structure's base by using finite element software environments.

Time history history analysis is a powerful numerical which tool that can provide a structural model response in the time domain to a specific earthquake ground motion

accelerogram [49]. The main advantages of the time history analysis are that it provides a time-dependent history of the structure's responses to a specific ground motion input, providing detailed information about the structure's stress and strain states over the response period. Path-dependent effects such as damping can be computed based on history responses [50].

The analysis is carried out at each incremental time interval and structural responses are evaluated at each time step. The method consists of a step-by-step direct integration in which the time domain is divided into many small time increments δt. At each time interval, the equations of motion are solved with displacements and velocities of the previous step serving as initial functions. Integration of time acceleration history gives the velocity history, integration of which, in turn, gives the displacement history [51].

Details of the input data of seismic actions used in the studied models are shown in Table 5.

Table 5. Input data of recorded Vrancea earthquakes accelerograms [47].

Earthquake Year	Peak Acceleration [m/s^2]	Total Duration [sec]	No. of Points	Spaced Interval	Damping [%]
1977	1.94927	40.14	2008	0.02	5
1986	0.66900	47.98	9596	0.005	5
1990	9.58×10^{-3}	52.9	9870	0.005	5

4. Results and Discussion

4.1. Modal Analysis Results

The modal shapes are shown in Figure 13. It can be observed that the first two modes are translational, having the periods of vibration and modal participating mass ratios given in Table 6. The fundamental period of vibration of the model solved by using the hand calculations shown in the P100-3/2019 code is empirically evaluated based on the number of levels, and is equal to 0.251 s. This value is closer to the fundamental period of vibration of the non-linear 3D model with frictionless contact between the spandrel and piers, as seen in Table 6.

The dynamic analysis results show that in both modeling cases, approaching the link between spandrels and piers contributes to the overall stiffness and dynamic behavior of the masonry structure. In post-earthquake damaged buildings, the separation between spandrels and piers can lead to a more flexible structure and also to the most unfavorable stress distribution in the element structure. The 2D linear shell model with the spandrel replaced by a hinged rigid link body has the most increased fundamental period, followed by the 3D solid non-linear–frictionless model. The presence of spandrel 3D solid elements affects the stiffness of the structure.

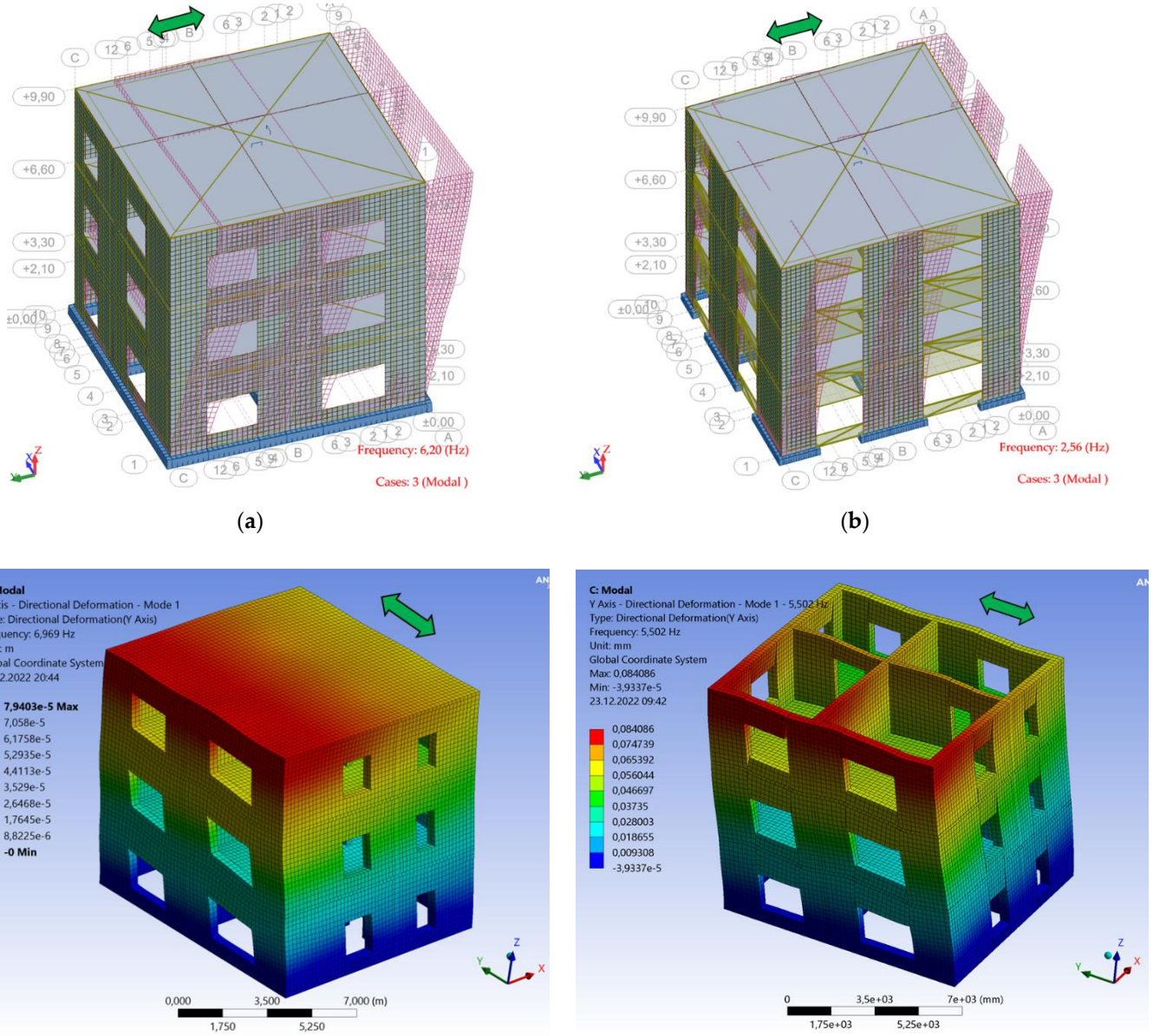
4.2. Time History Analysis Results in Terms of Stresses

Figure 14 shows the stress distribution versus time for the 3D solid analyzed models for seismic action recorded in Bucharest in 1977, 1986, and 1990.

Figures 15–17 show the von Mises stress distribution maps for the 2D linear shell model and the 3D solid non-linear model.

A comparison of the results for the seismic action recorded in Bucharest in 1977 shows that the maximum values obtained are similarly distributed. For the 2D linear shell model with rigid links, the maximum value of the von Mises stress is located at the base of the central wall near the door hole because this element is the stiffer and thicker one in the overall structure. The same location is observed for the 3D solid model with frictionless contacts.

For the seismic action recorded in Bucharest in 1986, the values of the von Mises stress are smaller than the previous seismic action. Moreover, for Bucharest 1990, the values are closer to Bucharest 1986 due to the close level of accelerations. Figure 18 shows a comparative graph for the maximum von Mises stress values.



(**a**) (**b**)

(**c**) (**d**)

Figure 13. Modal shapes in first mode of vibration: (**a**) 2D shell linear model—bonded; (**b**) 2D shell linear model—rigid; (**c**) 3D solid model–bonded; (**d**) 3D solid model—frictionless.

Table 6. Dynamic characteristics for the analyzed models.

Numerical Model	Mode	Period [s]	Frequency [Hz]	Modal Participating Mass Ratio on X Direction	Modal Participating Mass Ratio on Y Direction
2D-L-B	1	0.16	6.20	0.001	0.7698
2D-L-R	1	0.39	2.56	0.002	0.6514
3D-NL-B	1	0.14	6.969	0.00073	0.746
3D-NL-F	1	0.18	5.502	0.0014	0.722

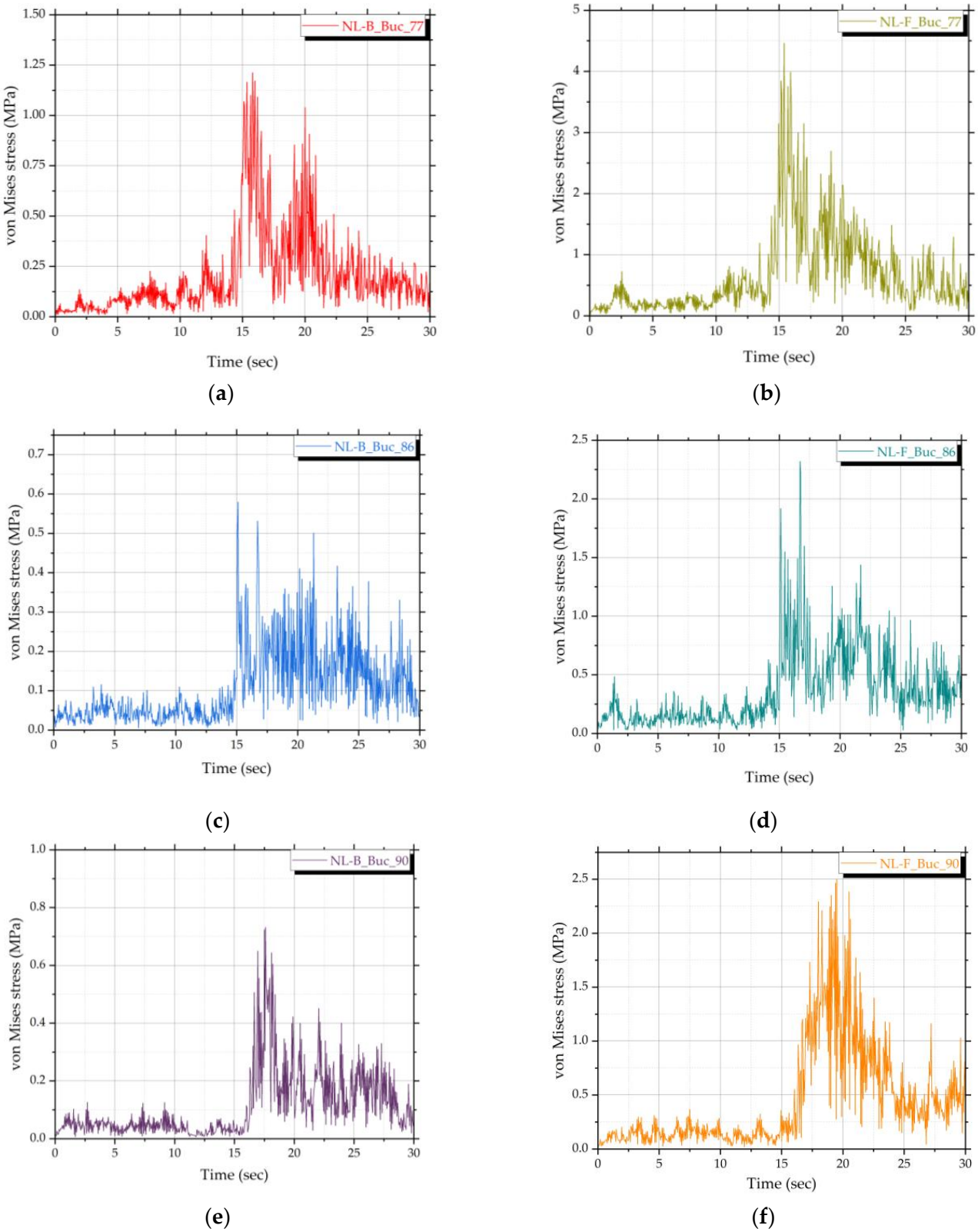
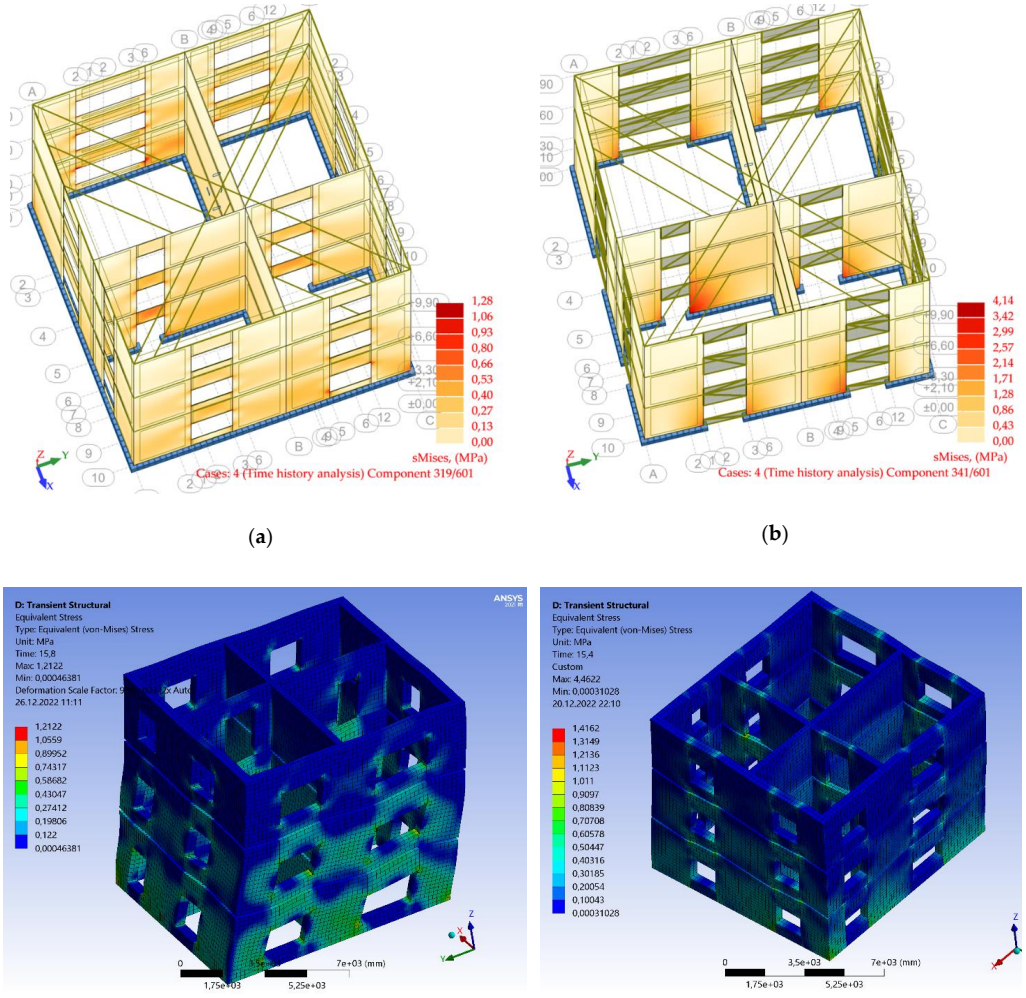


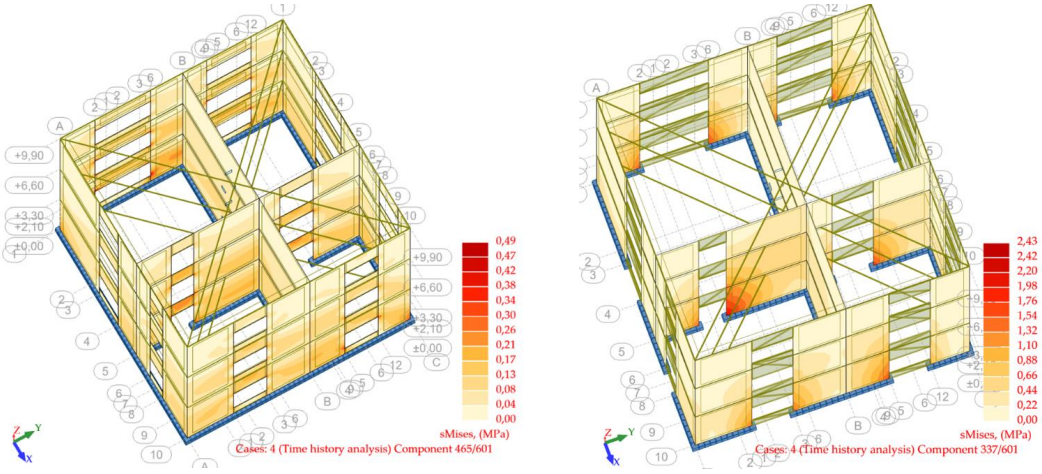
Figure 14. Von Mises stress distribution vs. time for 3D solid models: (**a**) 3D solid non-linear—bonded, Bucharest 1977; (**b**) 3D solid non-linear—frictionless, Bucharest 1977; (**c**) 3D solid non-linear—bonded, Bucharest 1986; (**d**) 3D solid non-linear—frictionless, Bucharest 1986; (**e**) 3D solid non-linear—bonded, Bucharest 1990; (**f**) 3D solid non-linear—frictionless, Bucharest 1990.



(**a**) (**b**)

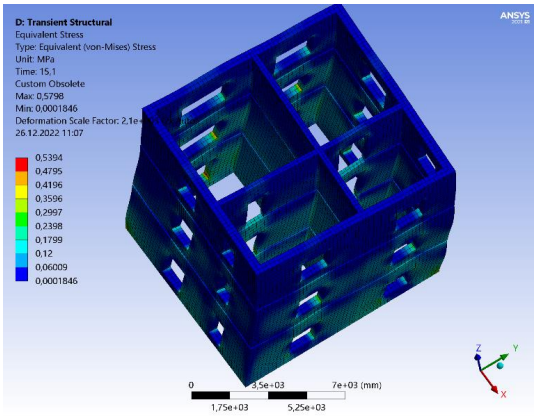
(**c**) (**d**)

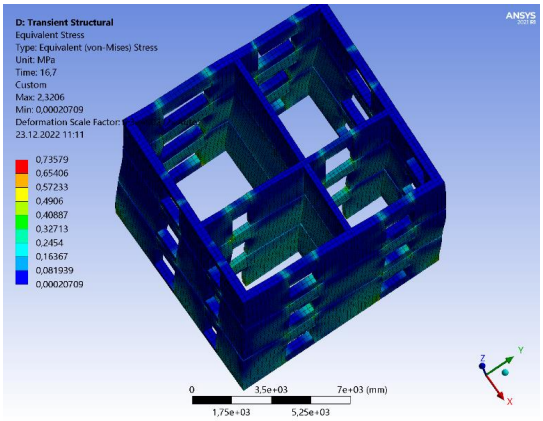
Figure 15. Von Mises stress distribution for the seismic action recorded in Bucharest in 1977: (**a**) 2D linear shell model—bonded; (**b**) 2D linear shell model—rigid; (**c**) 3D solid model—bonded; (**d**) 3D solid model—frictionless.



(**a**) (**b**)

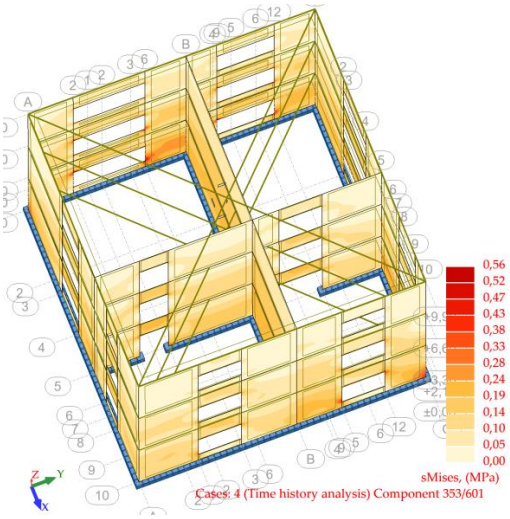
Figure 16. *Cont.*

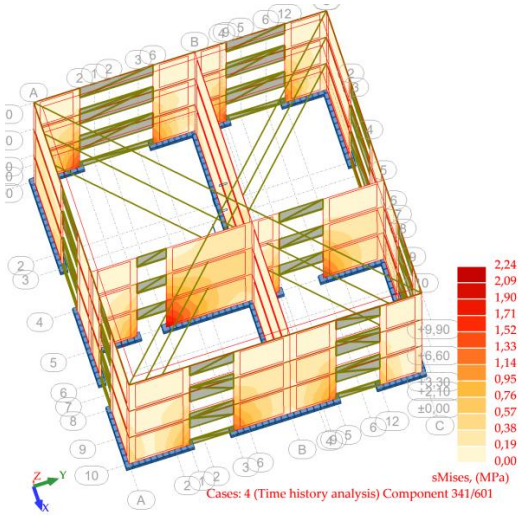




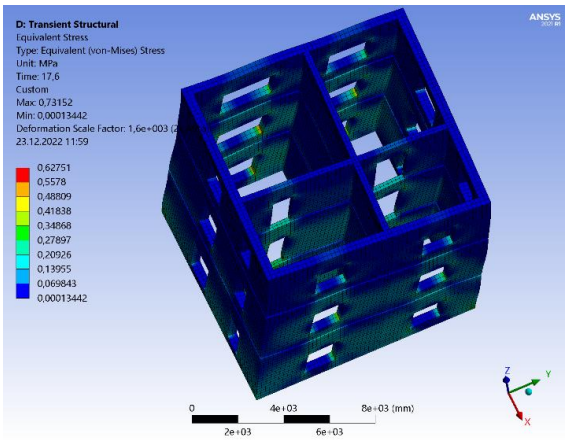
(**c**) (**d**)

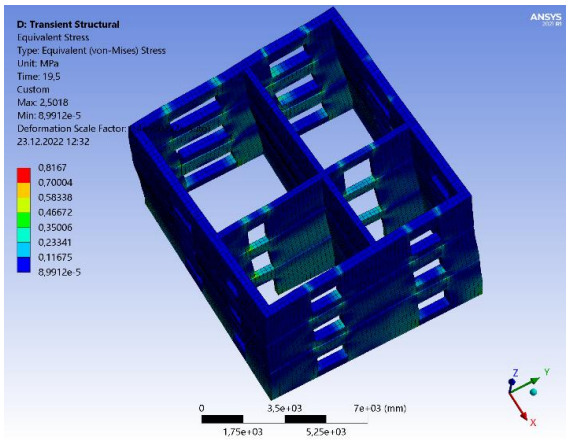
Figure 16. Von Mises stress distribution for the seismic action recorded in Bucharest in 1986: (**a**) 2D linear shell model—bonded; (**b**) 2D linear shell model—rigid; (**c**) 3D solid model—bonded; (**d**) 3D solid model—frictionless.





(**a**) (**b**)





(**c**) (**d**)

Figure 17. Von Mises stress distribution for the seismic action recorded in Bucharest in 1990: (**a**) 2D linear shell model—bonded; (**b**) 2D linear shell model—rigid; (**c**) 3D solid model—bonded; (**d**) 3D solid model—frictionless.

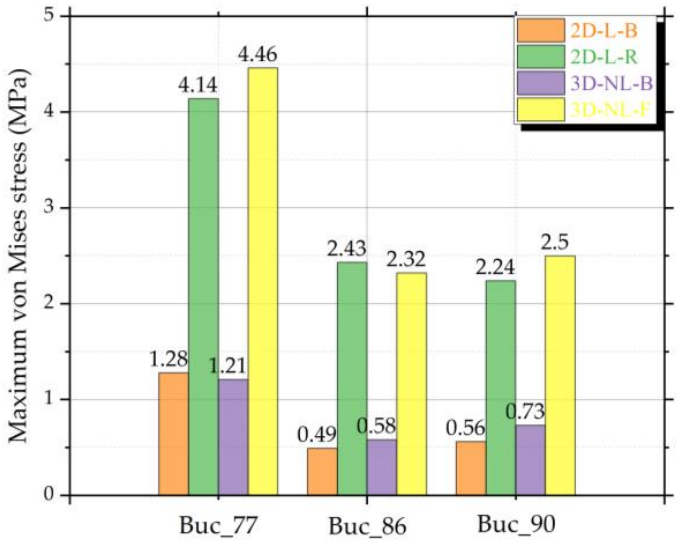


Figure 18. Von Mises stress comparison between time history analyses.

4.3. Time History Analysis Results in Terms of Displacements

Figure 19 presents the displacement versus time graph for the analyzed models in case of Bucharest 1977, 1986, and 1990 recorded seismic action.

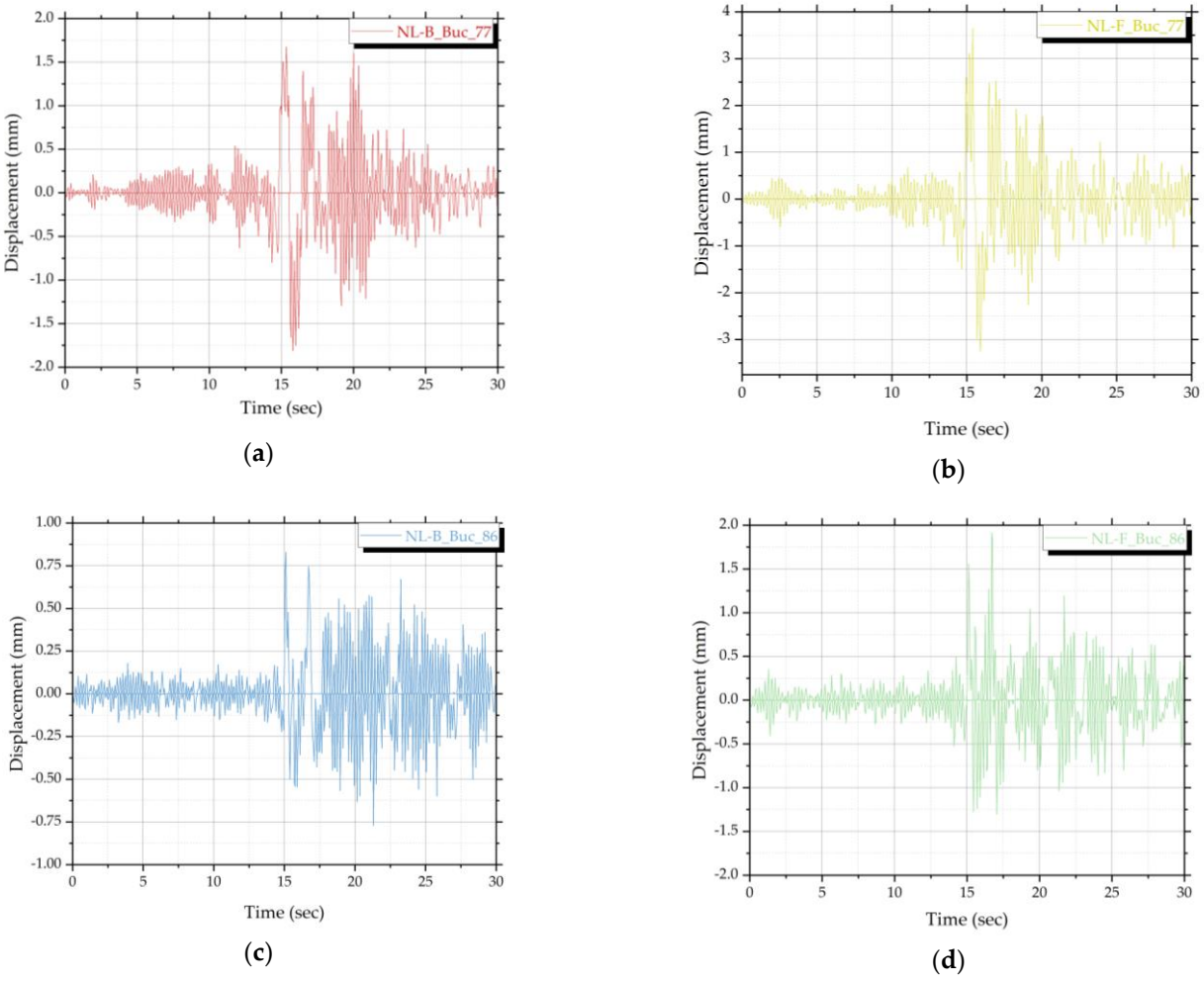
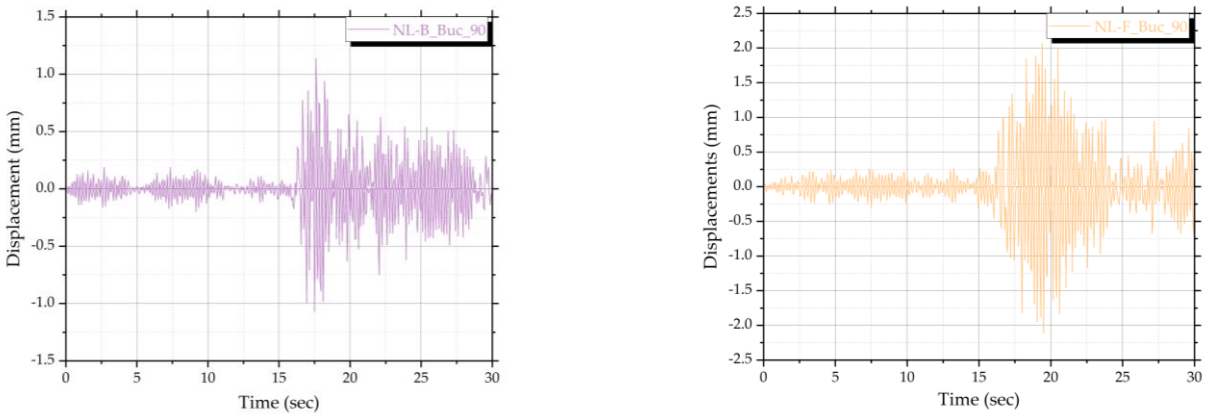


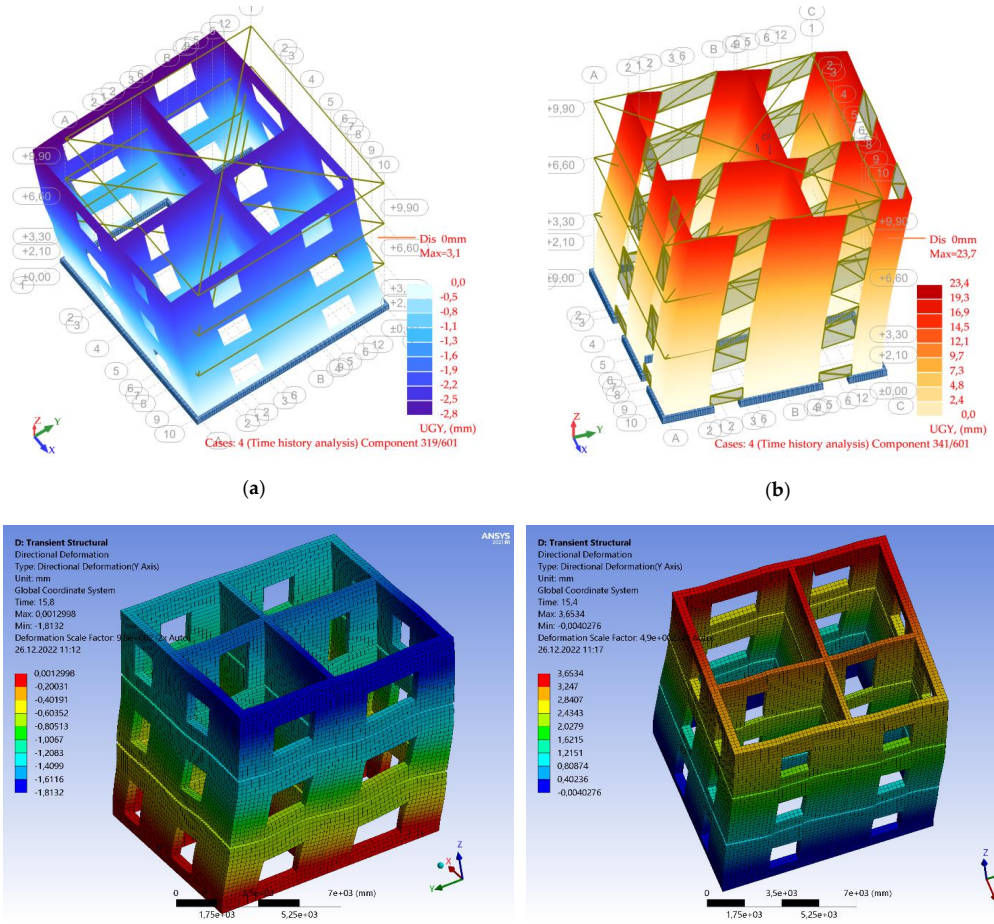
Figure 19. *Cont.*



(**e**) (**f**)

Figure 19. Von Mises stress distribution vs. time for 3D solid models: (**a**) 3D solid non-linear—bonded, Bucharest 1977; (**b**) 3D solid non-linear—frictionless, Bucharest 1977; (**c**) 3D solid non-linear—bonded, Bucharest 1986; (**d**) 3D solid non-linear—frictionless, Bucharest 1986; (**e**) 3D solid non-linear—bonded, Bucharest 1990; (**f**) 3D solid non-linear—frictionless, Bucharest 1990.

Figures 20–22 show the deformed shape of the analyzed models and the maximum displacement values from time history analyses.



(**a**) (**b**)

(**c**) (**d**)

Figure 20. Displacement distribution map for the seismic action recorded in Bucharest in 1977: (**a**) 2D linear shell model—bonded; (**b**) 2D linear shell model—rigid; (**c**) 3D solid model—bonded; (**d**) 3D solid model—frictionless.

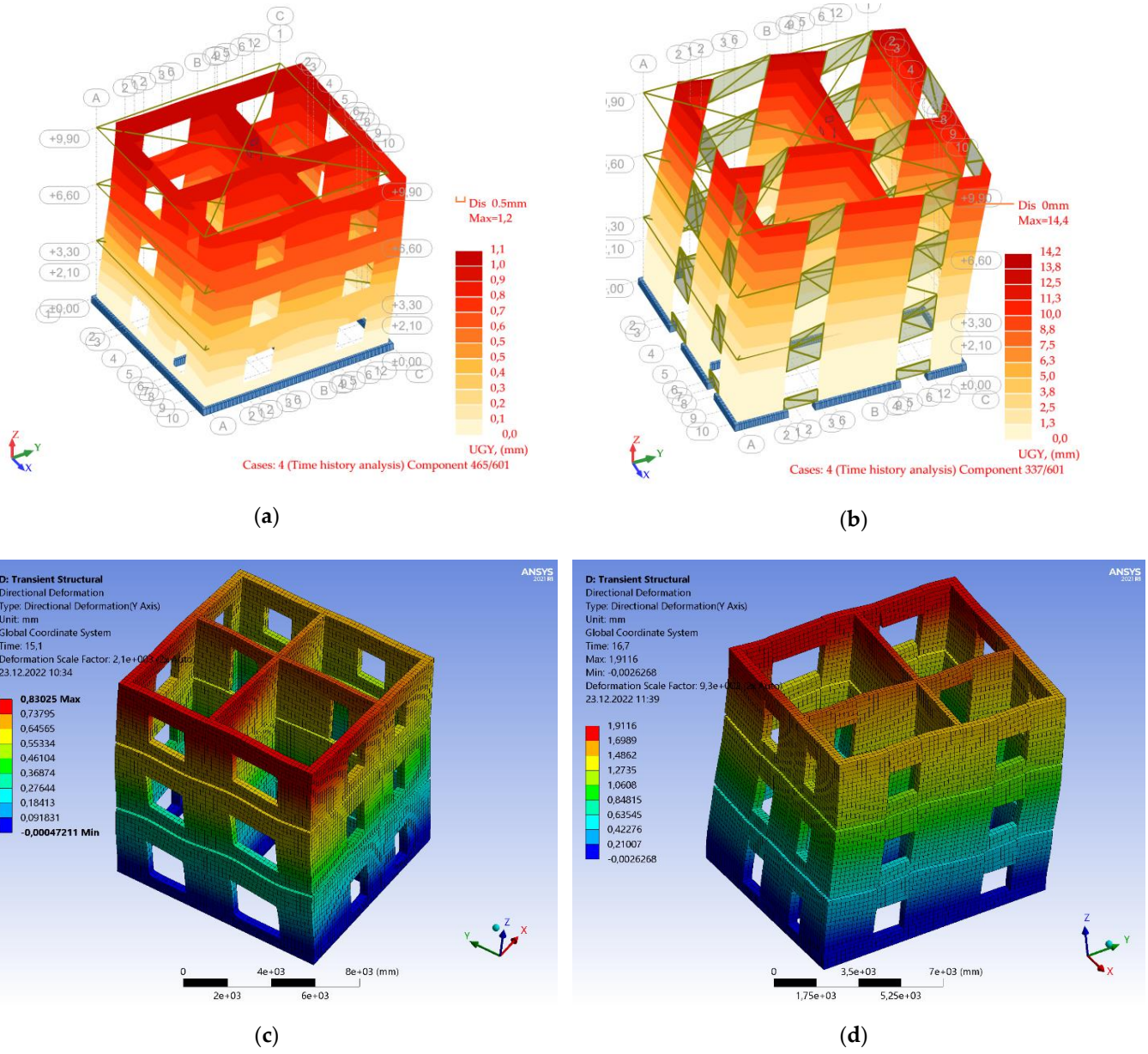


Figure 21. Displacement distribution map for the seismic action recorded in Bucharest in 1986: (**a**) 2D linear shell model—bonded; (**b**) 2D linear shell model—rigid; (**c**) 3D solid model—bonded; (**d**) 3D solid model—frictionless.

A comparison of the maximum absolute Y-direction displacements for both 2D shell and 3D solid model types, under the three inputs, is shown in Figure 23. The displayed values are under the seismic combination on the Y direction, as this is the weakest axis of the building.

The story displacement values obtained for the 2D linear shell model with rigid links are approximately 8 times larger in comparison with the others for the 1977 earthquake, and at least 13 times larger for the 1986 and 1990 earthquakes. The reason for this difference lies in the lack of flexural rigidity of the linear spandrels and their complete absence. These spandrels are only subjected to compression forces between adjacent piers. Therefore, the piers fully carry the bending moments and shear forces. There is no redistribution of bending moments between vertical structural elements, and for this reason, the design internal forces are larger for the 2D shell model with rigid links instead of spandrel elements. This can also be observed in the results shown in Tables 7–13.

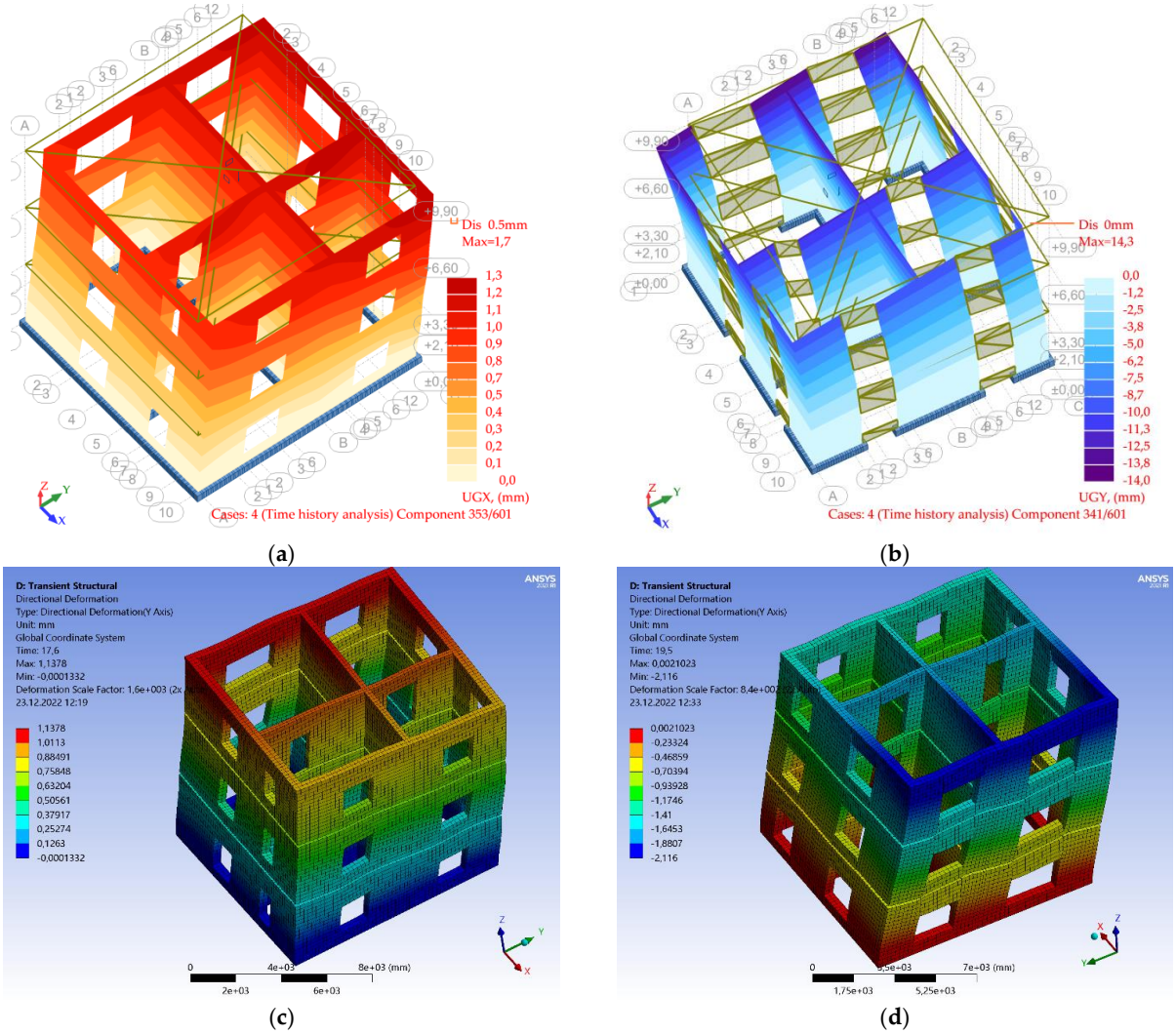


Figure 22. Displacement distribution map for the seismic action recorded in Bucharest in 1990: (**a**) 2D linear shell model—bonded; (**b**) 2D linear shell model—rigid; (**c**) 3D solid model—bonded; (**d**) 3D solid model—frictionless.

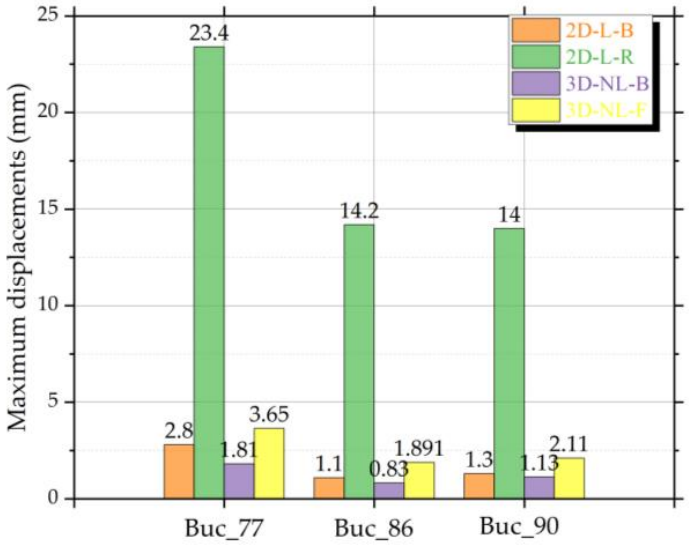


Figure 23. Maximum absolute displacement comparative graph.

Tables 7–13 present the pier internal design forces, shear capacity, R_3 indicator, and seismic risk class for each model obtained from all three recorded earthquakes and hand calculations.

Even though there is no difference in the risk class for the 1977 and 1986 earthquakes, the results show that the R_3 indicator of the linear spandrel model decreased by 10% and 26%, respectively. For the 1990 earthquake, the risk classes are very different; the risk class for the shell spandrel model is Rs IV and the risk class for the linear spandrel model is Rs II, in which case the reduction is 48%. This difference represents a safe construction in the event of a severe earthquake according to design codes (risk class Rs IV) compared to a structure at risk of collapse (risk class Rs II), the latter requiring structural rehabilitation. Furthermore, the results presented in P100-3/2019, obtained after manual calculations of the structure analyzed in this paper, classify the structure into seismic risk class Rs I with $R_3 = 0.25$. The reduction between the shell spandrel model R_3 indicator and manual calculations is 72%. This difference highlights the conservative nature of the design codes, which implies excessive structural rehabilitation demands.

Table 7. Seismic risk class assessment according to P100-3/2019 for the shell spandrel model from 1977 Vrancea earthquake input.

Pier	Load Combo	N_d kN	V_{Ed} kN	M_d kNm	V_{f1} kN	V_{f2min} kN	V_{Rd} kN	$R3_i$
T1	GSY	−238.7	34.359	37.585	107.16	52.842	52.842	1.5379
T2	GSY	−452.4	93.901	138.04	265.2	96.811	96.811	1.031
T3	GSY	−245.6	49.703	50.712	109.63	53.534	53.534	1.0771
T4	GSY	−153.2	17.391	20.931	69.314	34.631	34.631	1.9913
T5	GSY	−495.3	89.91	161.86	457.98	137.61	137.61	1.5305
T6	GSY	−202.1	34.27	37.309	116.44	46.587	46.587	1.3594
T7	GSY	−223	25.557	21.418	135.22	60.908	60.908	2.3833
T8	GSY	−466	75.102	125.63	411.98	155.35	155.35	2.0686
T9	GSY	−168.7	25.315	41.653	80.205	45.253	45.253	1.7876
L1	GSX	−469.8	59.736	74.211	454.55	162.64	162.64	2.7226
L2	GSX	−329.7	46.359	50.011	208.57	83.695	83.695	1.8054
L3	GSX	−166	27.966	36.663	79.114	44.942	44.942	1.607
L4	GSX	−174.2	14.891	17.522	76.726	36.715	36.715	2.4656
L5	GSX	−556.4	96.921	167.61	582.77	155.11	155.11	1.6004
L6	GSX	−147.2	23.479	20.519	67.093	34.009	34.009	1.4485
L7	GSX	−346.1	32.393	30.262	246.15	100.83	100.83	3.1127
L8	GSX	−426.1	56.702	82.537	318.6	124.67	124.67	2.1988
L9	GSX	−117.8	10.223	17.933	40.442	32.131	32.131	3.1429
		R_{3T} = 1.53427 R_{3L} = 2.101445			R_3 =1.53427		Risk class RsIV	

Table 8. Seismic risk class assessment according to P100-3/2019 for the shell spandrel model from 1986 Vrancea earthquake input.

Pier	Load Combo	N_d kN	V_{Ed} kN	M_d kNm	V_{f1} kN	V_{f2min} kN	V_{Rd} kN	$R3_i$
T1	GSY	−239.3	35.572	38.29	107.38	52.903	52.903	1.4872
T2	GSY	−451.2	95.285	141.27	264.69	96.691	96.691	1.0147
T3	GSY	−243.8	50.832	51.386	108.98	53.353	53.353	1.0496
T4	GSY	−152.8	16.283	20.013	69.159	34.588	34.588	2.1241
T5	GSY	−495.4	85.6	157.09	458.01	137.62	137.62	1.6067
T6	GSY	−204.2	32.553	35.895	117.4	46.807	46.807	1.4378
T7	GSY	−218	21.808	19.138	132.59	60.304	60.304	2.7651
T8	GSY	−464.7	67.786	117.47	411.07	155.16	155.16	2.2889
T9	GSY	−164.9	23.128	40.334	78.653	44.81	44.81	1.9374

Table 8. *Cont.*

Pier	Load Combo	N_d kN	V_{Ed} kN	M_d kNm	V_{f1} kN	V_{f2min} kN	V_{Rd} kN	$R3_i$
L1	GSX	−467.3	55.545	71.296	452.52	162.23	162.23	2.9208
L2	GSX	−329.3	44.195	47.998	208.4	83.658	83.658	1.8929
L3	GSX	−166.7	26.761	35.973	79.404	45.025	45.025	1.6825
L4	GSX	−173.8	14.017	16.836	76.579	36.674	36.674	2.6162
L5	GSX	−556	93.282	163.70	582.47	155.06	155.06	1.6622
L6	GSX	−148.6	22.591	19.845	67.611	34.154	34.154	1.5118
L7	GSX	−345.3	31.125	29.199	245.69	100.73	100.73	3.2361
L8	GSX	−425.7	55.096	81.327	318.34	124.61	124.61	2.2618
L9	GSX	−117.1	9.9959	17.790	40.211	32.039	32.039	3.2052
		R_{3T} = 1.59063 R_{3L} = 2.19556				R_3 = 1.59063		Risk class RsIV

Table 9. Seismic risk class assessment according to P100-3/2019 for the shell spandrel model from 1990 Vrancea earthquake input.

Pier	Load Combo	N_d kN	V_{Ed} kN	M_d kNm	V_{f1} kN	V_{f2min} kN	V_{Rd} kN	$R3_i$
T1	GSY	−227.8	64.85	68.83	103.1	51.73	51.730	0.797
T2	GSY	−442.8	157.1	234.8	261.1	95.850	95.850	0.609
T3	GSY	−237.3	80.11	81.41	106.6	52.70	52.703	0.657
T4	GSY	−150.07	31.14	35.01	68.14	34.304	34.304	1.101
T5	GSY	−488.4	145	273.8	453.5	136.713	136.71	0.942
T6	GSY	−192.31	52.30	61.93	111.8	45.5482	45.548	0.870
T7	GSY	−188.20	44.64	49.54	116.6	56.5789	56.578	1.267
T8	GSY	−456.71	117.5	201.5	405.3	153.937	153.93	1.309
T9	GSY	−128.80	36.54	57.20	63.19	40.2977	40.297	1.102
L1	GSX	−435.52	99.49	147.8	427.0	157.184	157.18	1.579
L2	GSX	−323.76	68.95	79.58	205.5	83.0144	83.014	1.203
L3	GSX	−143.07	39.73	48.70	69.41	42.1377	42.137	1.060
L4	GSX	−169.05	24.08	28.51	74.94	36.2124	36.212	1.503
L5	GSX	−537.33	145.3	282.7	568.6	152.614	152.61	1.050
L6	GSX	−145.53	34.10	31.54	66.46	33.833	33.833	0.992
L7	GSX	−327.63	58.86	69.23	235.3	98.377	98.377	1.671
L8	GSX	−420.64	86.93	134.3	315.3	123.937	123.93	1.425
L9	GSX	−103.75	15.69	23.39	36.16	30.411	30.411	1.937
		R_{3T} = 0.91535 R_{3L} = 1.32193				R_3 = 0.91535		Risk class RsIV

Table 10. Seismic risk class assessment according to P100-3/2019 for the linear spandrel model from 1977 Vrancea earthquake input.

Pier	Load Combo	N_d kN	V_{Ed} kN	M_d kNm	V_{f1} kN	V_{f2min} kN	V_{Rd} kN	$R3_i$
T1	GSY	−71.72	36.943	58.725	36.735	11.731	11.731	0.3175
T2	GSY	−366.9	62.793	223.4	226.96	87.884	87.884	1.3996
T3	GSY	−90.54	30.765	63.959	45.733	14.811	14.811	0.4814
T4	GSY	−97.67	20.645	33.115	47.261	28.379	28.379	1.3746
T5	GSY	−456.1	101.59	315.91	431.85	132.42	132.42	1.3035
T6	GSY	−139.3	35.815	59.212	85.229	39.47	39.47	1.1021
T7	GSY	−192.1	25.259	43.538	118.76	57.084	57.084	2.26
T8	GSY	−420.8	71.91	199.61	379.24	148.35	148.35	2.063
T9	GSY	−122	17.755	45.817	60.147	39.384	39.384	2.2182

Table 10. *Cont.*

Pier	Load Combo	N_d kN	V_{Ed} kN	M_d kNm	V_{f1} kN	V_{f2min} kN	V_{Rd} kN	$R3_i$
L1	GSX	−441.9	78.313	167.06	432.22	158.22	158.22	2.0203
L2	GSX	−297.6	42.773	77.403	191.92	79.922	79.922	1.8685
L3	GSX	−159.5	24.211	41.718	76.413	44.167	44.167	1.8242
L4	GSX	−126.5	17.853	27.705	59.131	31.774	31.774	1.7798
L5	GSX	−538.5	111.44	326.13	569.52	152.77	152.77	1.3709
L6	GSX	−104.8	18.262	26.619	50.284	29.255	29.255	1.602
L7	GSX	−315.3	42.122	76.665	227.98	96.707	96.707	2.2959
L8	GSX	−386	55.798	140.07	294.44	119.18	119.18	2.136
L9	GSX	−110.5	7.8918	17.913	38.235	31.248	31.248	3.9595
		R_{3T} = 1.38674 R_{3L} = 1.86434			R_3 = 1.38674		Risk class RsIV	

Table 11. Seismic risk class assessment according to P100-3/2019 for the linear spandrel model from 1986 Vrancea earthquake input.

Pier	Load Combo	N_d kN	V_{Ed} kN	M_d kNm	V_{f1} kN	V_{f2min} kN	V_{Rd} kN	$R3_i$
T1	GSY	−93.45	44.607	71.304	47.1	15.287	15.287	0.3427
T2	GSY	−358.5	73.021	271.45	222.92	54.538	54.538	0.7469
T3	GSY	−46.33	38.515	76.594	24.175	7.5782	7.5782	0.1968
T4	GSY	−103.4	22.42	36.421	49.685	29.082	29.082	1.2971
T5	GSY	−448.3	109.8	356.52	426.48	131.38	131.38	1.1965
T6	GSY	−131.8	38.257	65.985	81.192	38.53	38.53	1.0071
T7	GSY	−168.6	22.474	47.338	105.74	53.992	53.992	2.4024
T8	GSY	−418.1	69.725	205.78	377.21	147.92	147.92	2.1215
T9	GSY	−129.1	16.011	47.72	63.308	40.332	40.332	2.5191
L1	GSX	−439.6	64.487	141.87	430.29	157.83	157.83	2.4475
L2	GSX	−294.3	36.795	66.837	190.12	79.514	79.514	2.161
L3	GSX	−157.8	20.946	37.999	75.678	43.955	43.955	2.0985
L4	GSX	−133.8	15.274	24.252	61.98	32.575	32.575	2.1328
L5	GSX	−543.4	97.423	286.85	573.19	153.41	153.41	1.5747
L6	GSX	−110	15.62	23.184	52.449	29.877	29.877	1.9128
L7	GSX	−314.6	35.6	65.57	227.51	96.6	96.6	2.7135
L8	GSX	−382.6	48.967	124.95	292.38	118.72	118.72	2.4245
L9	GSX	−111.6	6.8775	16.759	38.573	31.384	31.384	4.5632
		R_{3T} = 1.19273 R_{3L} = 2.17513			R_3 = 1.19273		Risk class RsIV	

Table 12. Seismic risk class assessment according to P100-3/2019 for the linear spandrel model from 1990 Vrancea earthquake input.

Pier	Load Combo	N_d kN	V_{Ed} kN	M_d kNm	V_{f1} kN	V_{f2min} kN	V_{Rd} kN	$R3_i$
T1	GSY	120.27	75.719	124.23	59.391	19.673	19.673	0.2598
T2	GSY	−322	123.94	465.17	204.68	52.679	52.679	0.425
T3	GSY	92.971	69.868	129.72	46.873	15.208	15.208	0.2177
T4	GSY	−44.71	36.741	59.344	22.979	7.3131	7.3131	0.199
T5	GSY	−408.1	177.07	595.65	397.52	66.752	66.752	0.377
T6	GSY	−82.31	60.748	110.79	53.017	13.464	13.464	0.2216
T7	GSY	−108.5	31.906	84.892	70.484	17.743	17.743	0.5561
T8	GSY	−385.2	100.62	312.39	352.31	142.59	142.59	1.4171
T9	GSY	−15.58	20.313	67.073	8.3103	2.5481	2.5481	0.1254

Table 12. *Cont.*

Pier	Load Combo	N_d kN	V_{Ed} kN	M_d kNm	V_{f1} kN	V_{f2min} kN	V_{Rd} kN	$R3_i$
L1	GSX	−424.3	123.72	275.11	417.83	155.36	155.36	1.2557
L2	GSX	−273.2	63.076	118.32	178.67	76.912	76.912	1.2194
L3	GSX	−120.5	34.279	57.096	59.506	39.19	39.19	1.1432
L4	GSX	−105.8	27.576	42.888	50.701	29.375	29.375	1.0652
L5	GSX	−505.1	166.37	523.93	543.81	146.85	146.85	0.8827
L6	GSX	−83.88	28.266	41.727	41.246	25.642	25.642	0.9072
L7	GSX	−295.6	71.656	138.11	215.92	93.963	93.963	1.3113
L8	GSX	−362.2	86.458	224.59	279.59	115.82	115.82	1.3396
L9	GSX	−98.56	13.039	23.952	34.55	29.751	29.751	2.2817
		R_{3T} = 0.48495 R_{3L} =1.16019			R_3 = 0.48495		Risk class RsII	

Table 13. Seismic risk class assessment according to P100-3/2019–hand calculations from Annex H.

Pier	Load Combo	V_{Ed} kN	V_{f1} kN	V_{f2min} kN	V_{Rd} kN	$R3_i$
T1	GSY	59.97	26.69	46.7	26.69	0.445
T2	GSY	134.97	57.5	74.1	57.5	0.426
T3	GSY	59.97	26.69	46.7	26.69	0.445
T4	GSY	53.43	17.42	30.3	17.42	0.326
T5	GSY	325	99.98	81.9	81.9	0.252
T6	GSY	95.61	28.78	39.1	28.78	0.301
T7	GSY	166.05	36.2	46.9	36.2	0.218
T8	GSY	364.28	94.36	81.6	81.6	0.224
T9	GSY	93.18	23.67	39.9	23.67	0.254
L1	GSX	418.93	108.23	86.3	86.3	0.206
L2	GSX	172.43	55.87	72.0	55.87	0.324
L3	GSX	77.61	23.67	39.9	23.67	0.305
L4	GSX	41.57	17.42	30.3	17.42	0.419
L5	GSX	324.12	127.91	92.7	92.7	0.286
L6	GSX	41.51	17.56	30.6	17.56	0.423
L7	GSX	144.37	53.85	57.2	53.85	0.373
L8	GSX	170.47	69.38	70.0	69.38	0.407
L9	GSX	21.67	12.22	28.7	12.22	0.564
		R_{3T} = 0.258 R_{3L} =0.257		R_3 = 0.257		Risk class RsI

5. Conclusions

Masonry structures are very difficult to assess for structural rehabilitation. The Romanian design codes presents hand calculation methods with many limitations, such as high volume of work, time-consuming, poor accuracy, overlooked errors, and so on.

Damage occurrence by earthquakes located at the interface between spandrels and piers requires an adequate numerical model in a reasonable manner affordable for ordinary designers. The transformation of the initial structural integrity is validated by experimental data and scientific research literature on past earthquakes. To achieve such a numerical model in the current study, spandrels were replaced by rigid body hinged connections in a 2D linear shell model and with frictionless contact in a 3D solid non-linear model. Time history analyses were performed using three accelerograms recorded during the 1977, 1986, and 1990 Romanian earthquakes. After each time history analysis, it was observed that the numerical model of the initial structure, treated as bonded, exhibited stress concentration at the spandrel corners with maximum values larger than the strength of the masonry. The second stage of the analysis ignores the bond between the spandrel and piers, considering the links damaged, so the analyzed structure behaves very differently.

The results on the analysis show large variations between the two models, some of them making the difference in classifying a structure as either safe or under risk, which imposes some consolidation measures to ensure its strength and safety. A comparison is made between the results presented in this paper and the results of hand calculation provided by the Romanian design code P100-3/2019, which places the model in a risk class that is less favorable than the one obtained with the linear spandrel model. This was not surprising, as design codes are conceived to increase safety. Thus, the methods provided by these codes overestimate the actions applied to structures, usually resulting in unnecessary consolidation measures. This highlights the importance of using a model that best reflects reality and ensures the safety and time efficiency necessary to properly evaluate the structure.

However, this model presents some limitations, such as the fact that when modeling brick masonry as homogeneous, the behavior of spandrels depends on their geometry (slender vs. squat spandrels), undulations in the brick masonry, and the presence and type of lintels. The user of the proposed model should carefully assess the spandrel type and other parameters to model the structure correctly. In addition, using this type of modeling leads to more accurate results, resulting in more accurate consolidation solutions. This is reflected in cost and material efficiency, which, in turn, translates into sustainable consolidation solutions.

Author Contributions: Conceptualization, V.-M.V. and C.-P.N.; methodology, G.T.; software, V.-M.V., G.T.; validation, C.-P.N.; formal analysis, V.-M.V.; investigation, V.-M.V. and C.-P.N.; resources, V.-M.V.; data curation V.-M.V., G.T.; writing—original draft preparation, V.-M.V. and C.-P.N.; writing—review and editing C.-P.N., G.T., A.R.; visualization, C.-P.N.; supervision, V.-M.V., A.R.; project administration, V.-M.V.; funding acquisition, V.-M.V. and C.-P.N. All authors have read and agreed to the published version of the manuscript.

Funding: This research received no external funding. The APC was funded by the Erasmus+ project KA2–Higher education strategic partnerships no. 2018-1-RO01-KA203-049214, Rehabilitation of the Built Environment in the Context of Smart City and Sustainable Development Concepts for Knowledge Transfer and Lifelong Learning–RE-BUILT.

Institutional Review Board Statement: Not applicable.

Informed Consent Statement: Not applicable.

Data Availability Statement: Not applicable.

Conflicts of Interest: The authors declare no conflict of interest.

References

1. Jenkins, R.; Barton, J. *Environmental Regulation in the New Global Economy: The Impact of Industry and Competitiveness*; Edward Elgar Publishing: Cheltenham, UK, 2002.
2. KMB Energy Engineering Company Unveils 6 Fundamental Principles of Sustainable Building Design. Available online: https://www.kmbdg.com/news/energy-engineering-company-sustainable-building-design/ (accessed on 26 December 2022).
3. Almeida, C.P.; Ramos, A.F.; Silva, J.M. Sustainability Assessment of Building Rehabilitation Actions in Old Urban Centres. *Sustain. Cities Soc.* **2018**, *36*, 378–385. [CrossRef]
4. Almssad, A.; Almusaed, A.; Homod, R.Z. Masonry in the Context of Sustainable Buildings: A Review of the Brick Role in Architecture. *Sustainability* **2022**, *14*, 4734. [CrossRef]
5. Ministerul Dezvoltării, Lucrărilor Publice și Administrației. Masonry Structures Design Code—CR 6—2013. 2013. Available online: https://www.mdlpa.ro/userfiles/reglementari/Domeniul_V/V_9_3_CR_6_2013.pdf (accessed on 30 January 2023).
6. Cattari, S.; Beyer, K. Influence of Spandrel Modelling on the Seismic Assessment of Existing Masonry Buildings. In Proceedings of the Tenth Pacific Conference on Earthquake Engineering Building an Earthquake-Resilient Pacific, Sydney, Australia, 6–8 November 2015.
7. *FEMA 356*; Pre-Standard and Commentary for the Seismic Rehabilitation of Buildings. American Society of Civil Engineers: Reston, VA, USA, 2000.
8. Cattari, S.; Lagomarsino, S. A Strength Criterion for the Flexural Behaviour of Spandrel in Un-Reinforced Masonry Walls. In Proceedings of the 14th World Conference on Earthquake Engineering, Beijing, China, 12–17 October 2008.
9. Beyer, K.; Mangalathu, S. Review of Strength Models for Masonry Spandrels. *Bull. Earthq. Eng.* **2012**, *11*, 521–542. [CrossRef]
10. Beyer, K.; Dazio, A. Quasi-Static Cyclic Tests on Masonry Spandrels. *Earthq. Spectra* **2012**, *28*, 907–929. [CrossRef]

11. Beyer, K. Peak and Residual Strengths of Brick Masonry Spandrels. *Eng. Struct.* **2012**, *41*, 533–547. [CrossRef]
12. Dazio, A.; Beyer, K. Seismic Behaviour of Different Types of Masonry Spandrels. In Proceedings of the 4th European Conference on Earthquake Engineering, Ohrid, Macedonia, 30 August–3 September 2010.
13. Ahmad, N.; Ali, M. Displacement-Based Seismic Assessment of Masonry Buildings for Global and Local Failure Mechanisms. *Cogent Eng.* **2017**, *4*, 1414576. [CrossRef]
14. Guerrini, G.; Graziotti, F.; Penna, A.; Magenes, G. Improved Evaluation of Inelastic Displacement Demands for Short- Period Masonry Structures. *Earthq. Eng. Struct. Dyn.* **2017**, *46*, 1411–1430. [CrossRef]
15. Esposito, R.; Messali, F.; Ravenshorst, G.; Schipper, R.; Rots, J. Seismic Assessment of a Lab-Tested Two-Storey Unreinforced Masonry Dutch Terraced House. *Bull. Earthq. Eng.* **2019**, *17*, 4601–4623. [CrossRef]
16. Kim, G.-W.; Song, J.-K.; Jung, S.-J.; Song, Y.-H.; Yoon, T.-H. Lateral Load Distribution Factor for Modal Pushover Analysis. In Proceedings of the Council on Tall Buildings and Urban Habitat, Seoul, Republic of Korea, 10–13 October 2004.
17. Rostami, A.; Poursha, M. A Lateral Load Distribution for the Static Analysis of Base-Isolated Building Frames under the Effect of Far-Fault and near-Fault Ground Motions. *Structures* **2021**, *34*, 2384–2405. [CrossRef]
18. Quagliarini, E.; Maracchini, G.; Clementi, F. Uses and Limits of the Equivalent Frame Model on Existing Unreinforced Masonry Buildings for Assessing Their Seismic Risk: A Review. *J. Build. Eng.* **2017**, *10*, 166–182. [CrossRef]
19. Dumitraş, M.; Cobîrzan, N.; Dumitraş, D. Considerations Regarding the Analysis of Masonry Walls to Horizontal Loads Using Equivalent Frame Method Building. *Bull. Polytech. Inst. Jassy Constr. Archit. Sect.* **2013**, *59*, 41.
20. Gusella, F.; Orlando, M.; Thiele, K. Evaluation of Rack Connection Mechanical Properties by Means of the Component Method. *J. Constr. Steel Res.* **2018**, *149*, 207–224. [CrossRef]
21. Kasaeian, S.; Usefi, N.; Ronagh, H.; Dareshiry, S. Seismic Performance of CFS Strap-Braced Walls Using Capacity-Based Design Approach. *J. Constr. Steel Res.* **2020**, *174*, 106317. [CrossRef]
22. Soveja, L.; Budescu, M.; Gosav, I. Modelling Methods for Unreinforced Masonry Structures. *Bull. Polytech. Inst. Jassy Constr. Archit. Sect.* **2013**, *59*, 19.
23. Taranu, G. *Strengthening of Masonry Arches and Vaults at Historical Monuments/Consolidarea Arcelor si Boltilor din Zidarie la Monumentele Istorice*; Loghin, C., Ed.; Politehnium: Iasi, Romania, 2021; ISBN 978-973-621-497-4.
24. Pleşu, R.; Ţăranu, G.; Covatariu, D.; Grădinariu, I.-D. Strengthening and Rehabilitation Conventional Methods for Masonry Structures. *Bul. Inst. Politeh. Sect. Constr. Arhit.* **2011**, *57*, 165.
25. Venghiac, V.M.; Olariu, C.P.; Budescu, M. Structural Rehabilitation Analyses for a Romanian Cultural Heritage Building Located in Seismic Area. *Adv. Eng. Forum* **2017**, *21*, 196–203. [CrossRef]
26. Pleşu, R.; Taranu, G.; Budescu, M. FEM Analyses of a 1:2 Scale Historical Unreinforced Masonry Building. In Proceedings of the Computational Civil Engineering—CCE2013, International Symposium, Iasi, Romania, 24 May 2013.
27. Ple, R. Contributii Privind Metodele de Reabilitare a Structurilor din Zidarie/ Contributions Regarding the Rehabilitation Methods of Masonry Structures. Ph.D. Thesis, The "Gheorghe Asachi" Technical University of Iasi, Iasi, Romania, 2013.
28. Taranu, G.; Toma, I.-O.; Taranu, N. Shake Table Test of a 1:2 Scale Historical Unreinforced Masonry Building. In Proceedings of the 1st Croatian Conference on Earthquake ENgineering, 1 CroCEE, Zagreb, Croatia, 22–24 March 2021.
29. Ministerul Dezvoltării, Lucrărilor Publice și Administrației. Code for Earthquake Design P100-3/2019 Provisions for the Seismic Assessment of Existing Buildings 2019. Available online: https://www.mdlpa.ro/userfiles/reglementari/Domeniul_I/P100 partea%20a%20iiia.pdf (accessed on 14 January 2023).
30. Ansys | Engineering Simulation Software. Available online: https://www.ansys.com/ (accessed on 19 October 2021).
31. Robot Structural Analysis Professional. Available online: https://www.autodesk.com/products/robot-structural-analysis/overview (accessed on 13 January 2022).
32. Ansys Contact Types and Explanations. Available online: https://www.mechead.com/contact-types-and-behaviours-in-ansys/ (accessed on 14 January 2023).
33. Casapulla, C.; Portioli, F.; Maione, A.; Landolfo, R. A Macro-Block Model for in-Plane Loaded Masonry Walls with Non-Associative Coulomb Friction. *Meccanica* **2013**, *48*, 2107–2126. [CrossRef]
34. Sassu, M.; Andreini, M.; Casapulla, C.; de Falco, A. Archaeological Consolidation of UNESCO Masonry Structures in Oman: The Sumhuram Citadel of Khor Rori and the Al Balid Fortress. *Int. J. Arch. Herit.* **2012**, *7*, 339–374. [CrossRef]
35. Casapulla, C.; Argiento, L.U.; Maione, A.; Speranza, E. Upgraded Formulations for the Onset of Local Mechanisms in Multi-Storey Masonry Buildings Using Limit Analysis. *Structures* **2021**, *31*, 380–394. [CrossRef]
36. Casapulla, C.; Portioli, F. Experimental and Analytical Investigation on the Frictional Contact Behavior of 3D Masonry Block Assemblages. *Constr. Build. Mater.* **2015**, *78*, 126–143. [CrossRef]
37. Hafner, I.; Lazarević, D.; Kišiček, T.; Stepinac, M. Post-Earthquake Assessment of a Historical Masonry Building after the Zagreb Earthquake–Case Study. *Buildings* **2022**, *12*, 323. [CrossRef]
38. Croce, P.; Landi, F.; Puccini, B.; Martino, M.; Maneo, A. Parametric HBIM Procedure for the Structural Evaluation of Heritage Masonry Buildings. *Buildings* **2022**, *12*, 194. [CrossRef]
39. Manzini, C.F.; Ottonelli, D.; Degli Abbati, S.; Marano, C.; Cordasco, E.A. Modelling the Seismic Response of a 2-Storey URM Benchmark Case Study: Comparison among Different Equivalent Frame Models. *Bull. Earthq. Eng.* **2022**, *20*, 2045–2084. [CrossRef]

40. Croce, P.; Landi, F.; Formichi, P.; Beconcini, M.L.; Puccini, B.; Zotti, V. Non-Linear Methods for the Assessment of Seismic Vulnerability of Masonry Historical Buildings. In *Protection of Historical Constructions*; Lecture Notes in Civil Engineering; Springer: Cham, Switzerland, 2022; Volume 209.
41. Asad, M.; Zahra, T.; Thamboo, J.; Song, M. Finite Element Modelling of Reinforced Masonry Walls under Axial Compression. *Eng. Struct.* **2022**, *252*, 113594. [CrossRef]
42. Cannizzaro, F.; Castellazzi, G.; Grillanda, N.; Pantò, B.; Petracca, M. Modelling the Nonlinear Static Response of a 2-Storey URM Benchmark Case Study: Comparison among Different Modelling Strategies Using Two- and Three-Dimensional Elements. *Bull. Earthq. Eng.* **2022**, *20*, 2085–2114. [CrossRef]
43. Beconcini, M.L.; Formichi, P.; Giresini, L.; Landi, F.; Puccini, B.; Croce, P. Modeling Approaches for the Assessment of Seismic Vulnerability of Masonry Structures: The E-PUSH Program. *Buildings* **2022**, *12*, 346. [CrossRef]
44. Cattari, S.; Calderoni, B.; Caliò, I.; Camata, G.; de Miranda, S.; Magenes, G.; Milani, G.; Saetta, A. Nonlinear Modeling of the Seismic Response of Masonry Structures: Critical Review and Open Issues towards Engineering Practice. *Bull. Earthq. Eng.* **2022**, *20*, 1939–1997. [CrossRef]
45. D'Altri, A.M.; Cannizzaro, F.; Petracca, M.; Talledo, D.A. Nonlinear Modelling of the Seismic Response of Masonry Structures: Calibration Strategies. *Bull. Earthq. Eng.* **2022**, *20*, 1999–2043. [CrossRef]
46. *EN 1991-1-1*; European Committee for Standardization Eurocode 1: Actions on Structures—Part 1-1: General Actions—Densities, Self-Weight, Imposed Loads for Buildings. European Committee for Standardization: Brussels, Belgium, 2002.
47. INFP Bridging the Gap between Seismology and Earthquake Engineering: From the Seismicity of Romania towards a Refined Implementation of Seismic Action EN 1998-1 (2004) in Earthquake Resistant Design of Buildings (BIGSEES Project). Available online: http://bigsees.infp.ro/ (accessed on 26 December 2022).
48. *FEMA 450*; Building Seismic Safety Council of the National Institute of Building Sciences NEHRP. Recommended Provisions for Seismic Regulations for New Buildings and Other Structures, Part 1-15. Building Seismic Safety Council of the National Institute of Building Sciences NEHRP: Washington, DC, USA, 2003.
49. Chopra, A.K. *Dynamics of Structures*, 3rd ed.; Pearson Education: Noida, India, 2006.
50. Ministerul Dezvoltării, Lucrărilor Publice și Administrației. Romania P100-1/2013: Seismic Design Code—Part I: Design Rules for Buildings (in Romanian). 2013. Available online: https://www.mdlpa.ro/userfiles/reglementari/Domeniul_I/I_22_P100_1_2013.pdf (accessed on 26 January 2023). (In Romanian).
51. Hartmann, F.; Katz, C. *Structural Analysis with Finite Elements*; Springer: Berlin, Germany, 2007.

Disclaimer/Publisher's Note: The statements, opinions and data contained in all publications are solely those of the individual author(s) and contributor(s) and not of MDPI and/or the editor(s). MDPI and/or the editor(s) disclaim responsibility for any injury to people or property resulting from any ideas, methods, instructions or products referred to in the content.